Check for updates

Current progress in layered double hydroxide-based electrocatalysts for urea oxidation: insights into strategies and mechanisms

Asha K Satheesan, [iD] [ab] Ragunath Madhu, [iD] [ab] Sreenivasan Nagappan,[ab] Hariharan N Dhandapani, [iD] [ab] Aditi De, [iD] [ab] Suprobhat Singha Roy, [iD] [ab] Prasita Mazumder [iD] [ab] and Subrata Kundu [iD] *[ab]

The urea oxidation reaction (UOR) presents a more favorable alternative to the conventional oxygen evolution reaction (OER) for hydrogen production due to its lower thermodynamic potential. This method offers advantages over traditional hydrogen production approaches due to favorable operating conditions and potentially lower costs. However, the complex 6-electron transfer process in UOR limits its performance. Researchers are tackling this challenge by designing advanced electrocatalysts with optimized properties, such as porosity, heterostructures, controlled defects, surface functionalization, and fine-tuned electronic structures. This significant progress in UOR catalyst design holds promise for the future of clean energy technologies. In view of this, layered double hydroxides (LDHs) are attracting significant interest for their potential role in urea electrolysis due to the synergistic cooperation of metals, flexible configuration, tunable electronic composition and unique layered structure. This review examines the recent significant advancements in the design and synthesis of LDH-based UOR catalysts. Beyond highlighting recent breakthroughs in UOR catalysts, this review critically stresses the design strategies and challenges in urea electrolysis towards energy conversion. Moreover, this comprehensive approach provides a valuable forward-looking perspective on future research directions.

[a] *Materials Chemistry Laboratory for Energy, Environment and Catalysis, Electrochemical Process Engineering (EPE) Division, CSIR-Central Electrochemical Research Institute (CECRI), Karaikudi-630003, Tamil Nadu, India. E-mail: skundu@cecri.res.in, kundu.subrata@gmail.com; Tel: +914565-241487*
[b] *Academy of Scientific and Innovative Research (AcSIR), Ghaziabad-201002, India*

Asha K Satheesan received her B.Sc. degree from Sree Kerala Varma College, affiliated with the University of Calicut (2014–2017), and her M.Sc. degree in Physical Chemistry from Mahatma Gandhi University (2017–2019). She obtained her M.Phil. from Cochin University of Science and Technology. She has qualified for the CSIR–UGC NET (National Level Eligibility Test) and received a JRF (Junior Research fellowship) from CSIR, New Delhi. She has been pursuing her PhD under the guidance of Dr Subrata Kundu at CSIR-CECRI since January, 2024 and is working on electrocatalytic water splitting applications.

Asha K Satheesan

Ragunath Madhu received his B.Sc. degree (2014–2017) from the Gandhigram Rural Institute, Dindigul, India, and his M.Sc. degree in Analytical Chemistry from the University of Madras, Chennai, India (2017–2019). As he ranked at the top of his university during his M.Sc., he was awarded a gold medal and an INSPIRE scholarship (SRF) by DST, New Delhi, in March 2020. Ragunath Madhu joined Dr Subrata Kundu's research group in August 2020, and his PhD thesis work primarily focuses on catalysis, SERS, and electrocatalytic water splitting applications.

Ragunath Madhu

1. Introduction

The depletion of fossil fuels has gained interest in renewable energy technologies. Particular attention has focused on electrochemical processes like the oxygen evolution reaction (OER), hydrogen evolution reaction (HER), and urea oxidation reaction (UOR) is increasing owing to their potential for efficient and ecological energy production.[1–3] Among them, urea electrolysis offers a significant advantage by requiring a substantially lower potential of 0.37 V compared to the 1.23 V vs. RHE needed for water splitting. Furthermore, urea electrolysis offers several advantages, including minimal interference with hydrogen production and the potential to generate value-added products or degrade pollutants at the anode. It can potentially reduce the energy budget by up to 93%. Urea is an effective hydrogen-rich chemical fuel, with a hydrogen storage content of 6.67 wt% hydrogen. It consists of carbon (C), hydrogen (H_2), nitrogen (N_2), and oxygen (O_2), making it a viable alternative anodic fuel for fuel cells.[3–6] The abundance of urea is plentiful in (1) human urine (2–2.5 wt%, 0.33 mol L^{-1}) as a natural byproduct of animal and human metabolism to remove excess nitrogen from the body;[7,8] (2) urea-containing wastewater, as several methods, including adsorption, biological decomposition, oxidation, and catalytic decomposition, have been engaged to eliminate urea from wastewater; and (3) industrial wastewater, as urea is widely manufactured for fertilizers, melamine synthesis, and diesel additives. This offers multiple applications, such as a H_2 source, catalyst design, urea removal, and functioning within direct urea fuel cells (DUFCs).[9] Nevertheless, without proper treatment, urea can hydrolyze to ammonia, contributing to acid rain and environmental pollution.[10,11] Ammonia easily oxidizes to form harmful pollutants, including nitrite, nitrate, and nitrogen oxides, which penetrate soil and water, causing health risks. Direct emissions of urea into the environment also lead to substantial energy waste. Traditional urea treatments, such as adsorption, hydrolysis, chemical oxidation, and, biodegradation, are generally limited by high costs and extreme energy consumption, often necessitating

Sreenivasan Nagappan received his Bachelor of Science degree from Gobi Arts and Science College under Bharathiar University (2015–2018) and his Master of Science degree from Madras University (2018–2020) with a specialization in Inorganic Chemistry. As he ranked at the top of his university during his M.Sc., he was awarded a gold medal and an INSPIRE scholarship (JRF) by DST, New Delhi, in March 2021. Currently, he is pursuing his PhD under Dr Subrata Kundu's supervision since August 2021 in the field of "Electrospun Transition Metal-based Modified Nanofibers for Water Electrolysis".

Sreenivasan Nagappan

Hariharan N Dhandapani completed his Bachelor of Science degree from Sacred Heart College under Thiruvalluvar University (2012) and his Master of Science degree from Madurai Kamaraj University (2014) in General Chemistry. After qualifying for the NET (National Eligibility Test) and receiving a JRF (Junior Research Fellowship) from CSIR, New Delhi, with an all-India ranking of "87" (November 2020, Chemical Science), he joined Dr Subrata Kundu's research group in August 2021. He is currently working on his PhD thesis, mainly focusing on "Modified Transition Metal Double Layer Hydroxides for Water Splitting Applications".

Hariharan N Dhandapani

Aditi De received her Bachelor of Science degree from Bankura Christian College under The University of Burdwan (2017) and her Master of Science degree from West Bengal State University (2019) with a specialization in Organic Chemistry. She qualified for the WB-SET (West Bengal State Level Eligibility Test), the NET (National Eligibility Test), and the GATE (Graduate Aptitude Test in Engineering). She joined Dr Subrata Kundu's research group in April 2022 and is currently working towards her PhD thesis, mainly focusing on electrocatalytic water splitting applications.

Aditi De

Suprobhat Singha Roy received his B.Sc. degree (2016–2019) from Ramakrishna Mission Vivekananda Centenary College under West Bengal State University and his M.Sc. degree (2019–2021) from the School of Chemistry, University of Hyderabad. He qualified the joint CSIR-UGC NET examination in 2022 and was awarded the UGC-Junior Research Fellowship. He joined Dr Subrata Kundu's research group in August 2022, and his work mainly focuses on nanomaterials-based catalyst development for electrocatalytic water splitting applications.

Suprobhat Singha Roy

excessive temperatures that can inactivate biological enzymes. On the contrary, the UOR proposes simple operations, including large-scale processing with extended operation cycles and stable production of carbon dioxide (CO_2) and N_2 in a basic solution. Thus, urea electrolysis not only reduces energy consumption in H_2 production but also contributes to wastewater management. Nonetheless, the UOR at the anode is sluggish, demanding the growth of effective and inexpensive catalysts. Primarily, intensive research has focused on noble metals, but their expensiveness and scarcity have encouraged the search for low-cost alternatives. Recently, transition metal (Fe, Co, Ni, Mn, and Mo)-based catalysts including oxides, hydroxides, phosphides, sulfides, selenides, and nitrides show promising performance towards water splitting and UORs.[12–19] Transition metal-based layered double hydroxides (LDHs) and their derivatives stand out due to their abundance, affordability, and promising catalytic properties for water splitting.[20] Further, being made from earth-abundant elements, the LDH production is economically viable.[21] The LDHs are ion lamellar crystals composed of positively charged brucite-like layers and negatively charged interlayer anions (2D layered structure). Trivalent metal cations (*e.g.*, Fe^{3+}, Mn^{3+}, Al^{3+}, and Ga^{3+}) partially replace bivalent cations (*e.g.*, Co^{2+}, Ni^{2+}, and Fe^{2+}) in the octahedral coordination of hydroxyl groups, creating the positively charged layers. Interlayer anions (*e.g.*, CO_3^{2-}, NO_3^{-}, SO_4^{2-}, Cl^{-}, and RCO_2^{-}) balance the additional positive charge. Hydroxyl groups in the LDH layers face the interlayer region and may form hydrogen bonds with anions and water. The general LDH formula is $[M_{1-x}^{2+}M_x^{3+}(OH)^2][An^-]_{x/n}\cdot zH_2O$, where M^{2+}, M^{3+}, An^-, x, n, and z represent specific elements and stoichiometric ratios. This unique structure offers advantages such as tunable metal cations, adjustable interlayer anions, and exfoliation into ultrathin nanosheets.[22] LDHs favor the UOR by

their capability of boosting the reaction kinetics and robustness under mild conditions. The synergistic effects and redox properties of transition metals such as Ni, Fe, and Co exceptionally promote the LDH compounds as highly efficient catalysts for UORs.[23–26] The interlayer places in LDHs can be easily engineered to augment the diffusion of urea and its intermediates during reaction conditions, further progressing the catalytic performance.[27] Moreover, synergistic cooperation of metal cations and fine-tuned electronic structures with doping, surface modifications, and alloying demonstrates elevated urea oxidation efficiency over the years.[28–32] However, despite noteworthy advancements, lacking a comprehensive understanding of efficient LDH-based UOR catalysts restricts their industrial application, signifying the necessity for further study to optimize these systems. In this review, for the first time, we explore several LDH-based systems for UOR-coupled electrochemical water splitting (OER/HER). In addition, we explore various notorious LDH-based materials and their derivatives with the fabrication approach and electrocatalytic activity of the discussed catalysts. Afterward, the advancement and strategies for developing LDH-based catalysts for UORs are briefly discussed. Finally, a summary and outlook are deliberated with a hint of future developments in this area. As far as we can ascertain, this is the first instance of LDH-based catalysts for UOR applications that are thoroughly reviewed in this work, inspiring cutting-edge breakthroughs in green energy technologies while mitigating pollution.

2. The need of urea electrolysis

The generation of H_2 *via* water electrolysis powered by renewable energy sources is a primary concern of scientists worldwide. However, due to high energy input for the OER at the

Prasita Mazumder

Prasita Mazumder received her Bachelor of Science degree from Jadavpur University (2018–2021) and her Master of Science degree from Jadavpur University (2021–2023) with a specialization in Inorganic Chemistry. She was awarded an INSPIRE scholarship (JRF) in February 2024 by DST, New Delhi. Currently, she is pursuing her PhD under Dr Subrata Kundu's supervision since August 2024 in the field of "Functionalized Metal–Organic Frameworks as Noble Metal-Free Electrocatalysts for Water Splitting Applications".

Subrata Kundu

Dr Subrata Kundu received his PhD from the Indian Institute of Technology (IIT), Kharagpur, India in early 2005. He then moved to the University of Nebraska, Lincoln, USA, and later to Texas A&M University, College Station, Texas, USA, as a postdoctoral fellow (2005–2010). He is currently working as a Principal Scientist at CSIR-CECRI, Karaikudi, India. Dr Kundu has been serving as an associate editor for the prestigious 'Journal of Materials Chemistry A' and 'Materials Advances' from RSC Publishers since 2022, as well as for 'Scientific Reports' from the Nature Group Publishers since 2015. In 2023, Dr Kundu was honoured with the prestigious title of 'Fellow of the Royal Society of Chemistry (FRSC)' from London, UK. Dr Kundu and his co-workers are working at the forefront of material sciences, with a focus on energy, environment, catalysis and electrocatalysis applications.

anode, the process is not economically viable and is a challenge. The thermodynamic potential to split the water molecule into H_2 and O_2 is 1.23 V *vs*. RHE. In practice, additional energy is required to catalyze the OER and HER efficiently. The major concern is associated with the sluggish reaction kinetics of the OER process. Hence, the OER is considered the bottleneck of the process, resulting in an increase in the high energy input to generate H_2.[33] The energy efficiency is important for industrial applications. For an electrolysis cell (HER/OER) operating at 1.0 A cm^{-2} current density (a current density of practical interest), the requirement of cell voltage is roughly 1.8–2.0 V, which leads to energy conversion efficiency less than unity.[34] In fact, with the increase in applied voltage, this efficiency gets reduced further. Hence, the overall energy efficiency is less when H_2 is generated *via* water electrolysis. This factor has impact on its feasibility as a widespread energy solution. Therefore, it is necessary to increase the energy efficiency of hydrogen fuel by generating H_2 with low energy input. In view of this, the use of value-added anodic reactions (sacrificial agents), such as urea electrolysis, which oxidizes at a far lower potential than water, can serve as an attractive alternative to overcome the sluggish nature of the anodic process.[3,35–38] Hence, urea electrolysis is a promising alternative to water electrolysis due to its potential for lower operating potentials. This could not only enhance the energy efficiency but also mitigate catalyst degradation, a major concern in water electrolysis caused by the high anodic potentials required for oxygen evolution. Designing and developing suitable electrocatalysts for urea oxidation require low anodic potential, and thus, the electrocatalysts are expected to have a longer lifecycle.[3–5]

Similar to water electrolysis, H_2 production through urea electrolysis is also performed by applying electrical current *via* aqueous electrolytes (for example, KOH + urea) (Fig. 1a). The theoretical voltage of urea electrolysis in urea-assisted water splitting is only 0.37 V *vs*. RHE, whereas the voltage of water splitting is 1.23 V *vs*. RHE. This substantial difference in voltage requirements translates to significant energy savings in the H_2 production process (Fig. 1b).[35] The urea electrolysis is possible under acidic, neutral and alkaline pH conditions; however, the alkaline condition is mostly preferred especially for materials such as LDH.[39] Under acidic conditions, the material dissolution and therefore structural collapse are a major problem. Under neutral conditions, when NaCl is chosen as the electrolyte to simulate urine environment, Cl$^-$ from the electrolyte undergoes oxidation and yields Cl_2 molecules. Subsequently Cl_2 reacts with water to produce HOCl. Further, HOCl reacts with urea to produce N_2, CO_2, and hydrochloric acid (HCl). The produced H$^+$ creates localized acidity, and hence, the material stability is compromised.[5] Consequently, researchers often opt for alkaline media to study the UOR to avoid the aforementioned issues. Under alkaline conditions, the UOR at the anode (eqn (1)) requires a theoretical potential of −0.46 V *vs*. standard hydrogen electrode (SHE):

$$CO(NH_2)_2 + 6OH^- \rightarrow CO_2 + N_2 + 5H_2O + 6e^- \quad (1)$$
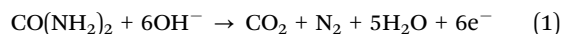
Then, the HER at the cathode (eqn (2)) requires a theoretical potential of −0.83 V *vs*. SHE:

$$6H_2O + 6e^- \rightarrow 3H_2 + 6OH^- \quad (2)$$
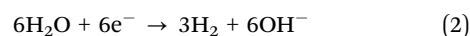
The overall urea electrolysis (eqn (3)) reaction requires a total theoretical cell voltage of 0.37 V *vs*. RHE:

$$CO(NH_2)_2 + H_2O \rightarrow 3H_2 + CO_2 + N_2 \quad (3)$$
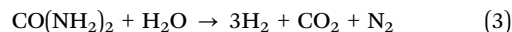
Therefore, the total urea-assisted water splitting requires only a voltage of 0.37 V *vs*. RHE, which is 0.86 V *vs*. RHE lower than the conventional water splitting process.[5,33]

Despite its lower potential than that of the OER, the UOR still presents opportunities for further research and development. Efforts to reduce the UOR potential and increase current density are ongoing. Additionally, the electrolysis of urea can be used to treat urea-rich wastewater, which is a cost-effective and ecofriendly method. Thus, this dual-purpose approach of urea electrolysis not only provides the solution for energy efficiency for H_2 production but also can be used to treat waste water, thereby benefiting society.[38,40,41]
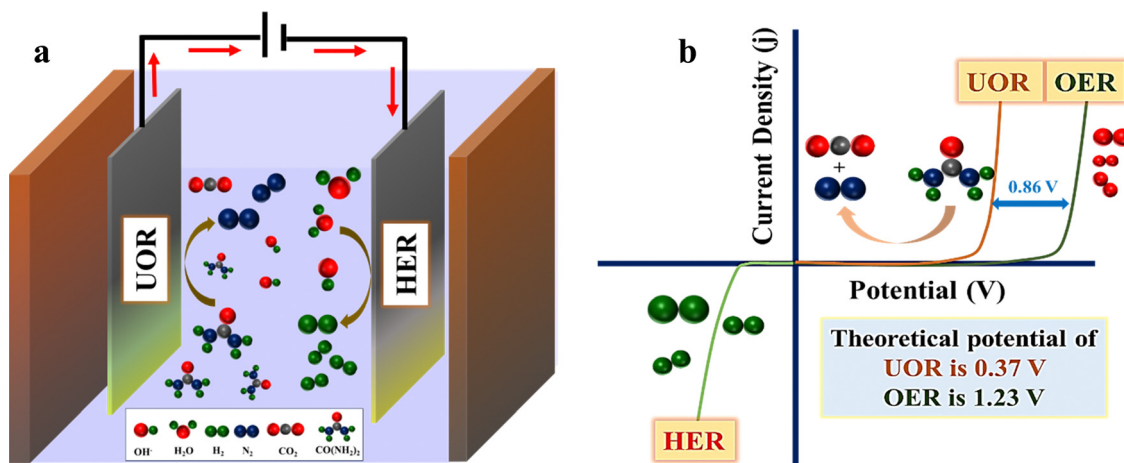

Fig. 1 (a) Schematic of urea-assisted water splitting (urea electrolysis) for hydrogen production. (b) Comparison of polarization curves for UOR, OER and HER.

3. Reaction mechanism of UOR

As mentioned above, compared to acidic and neutral environments, the UOR under alkaline conditions has several advantages such as negligible corrosion, reduced vulnerability to CO poisoning, and the opportunity for using more affordable non-precious electrocatalysts.[42,43] This further emphasizes the practical advantages of alkaline environments for the UOR. In 2010, Botte et al. established a most favorable possible reaction pathway for urea adsorption on surface-reconstructed NiOOH from Ni(OH)$_2$.[44] Initially, the urea molecule was adsorbed over the catalytic active site (Ni). Then, the urea molecule undergoes continuous deprotonation of the H–N–H bond by the OH$^-$ ions adsorbed onto C atoms, resulting in N$_2$ desorption (Pathway 1 and Pathway 2), as shown in Fig. 2. In an alternative pathway (Pathway 3), the amine group of urea separates from the C atom and attaches to the N–H group, forming a cyclic structure. This structural change favors the desorption pathway. The detailed discussion is expressed in the following section.

3.1. Pathway 1 and 2

In the initial step, the urea molecule is adsorbed onto the active sites of the metal catalyst to form a $[M \cdot CO(NH_2 \cdot NH_2)]_{ads}$ adduct. Then the OH$^-$ ion abstracts a proton from the $[M \cdot CO(NH_2 \cdot NH_2)]_{ads}$ adduct, and deprotonation of the amine group leads to the formation of $[M \cdot CO(NH_2 \cdot NH)]_{ads}$ followed by the release of electrons and water molecules. The formed adduct undergoes subsequent removal of protons continuously until all the protons are removed from the adduct leading to the formation of $[M \cdot CO(N_2)]_{ads}$. Further, the desorption of N$_2$ occurs through the reaction of OH$^-$ ions with $[M \cdot CO(N_2)]_{ads}$, followed by the formation of $[M \cdot CO_2]_{ads}$. In the final step, the CO$_2$ molecule gets desorbed from the metal's active sites, resulting in the reduction of the oxidation state of the metal.

3.2. Pathway 3

The initial step of pathway 3 occurs in a similar step to that of pathway 1 and 2 till the formation of $[M \cdot CO(NH_2 \cdot NH)]_{ads}$. Subsequently, the H–N–H amine group attached to the N–H group through the cyclic structure formation. Then deprotonation preferentially occurs on the H–N–H group, forming $[M \cdot CO(NH \cdot NH)]_{ads}$. The deprotonation will continue until the formation of $[M \cdot CO \cdot N_2]$. The following steps are similar to pathway 1 and 2. Due to the ease of formation of the N–N bond, the desorption of CO$_2$ from M^{n+} is more favorable in pathway 3, which can be considered as the rate-determining step.

4. Various routes of synthesis of LDHs

There are various techniques used for the LDH synthesis: (1) co-precipitation method; (2) urea hydrolysis; (3) hydrothermal synthesis; (4) sol–gel method; (5) microwave process etc. The co-precipitation method is a widely used technique for synthesizing various forms of LDHs. It involves the simultaneous precipitation of trivalent and divalent metal salts in an alkaline medium under constant pH, which controls the morphology and molecular size of LDHs. The pH is adjusted to more than 8 when titrating with 0.1 M NaOH to enhance the coprecipitation. After the precipitate was aged at room temperature for 24 h, it was washed with deionized water and vacuum-dried to obtain the product. The main advantages of this technique are simplicity, scalability, and cost-effectiveness. Miyata et al. used various parameters such as washing conditions, reactant concentrations, and pH for the synthesis of LDH.[45] In the urea hydrolysis method, urea can act as a weak Brønsted base and precipitating agent to improve the pH by thermal decomposition. Urea hydrolysis is a slow process that starts at 90 °C, which leads to an increase in pH up to 10 and the carbonate anions act as interlayer anions which form monodisperse LDH materials with high crystallinity and purity. In this method, the metal salt solutions of M^{2+} and M^{3+} are mixed with urea and heated at a moderate temperature of 120–180 °C, which results in ammonia release at a slow rate, which acts as a weak base, increasing the pH and facilitating precipitation. LDHs prepared from urea hydrolysis produce well-crystallized LDHs and are uniform with controlled morphology. Berber et al. reported the optimized conditions for the synthesis of LDHs by varying the urea
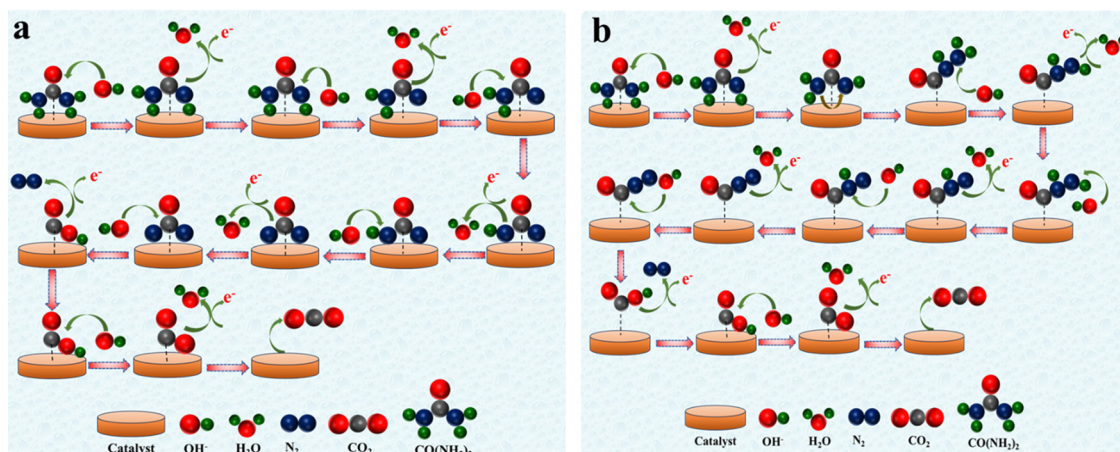

Fig. 2   Schematic of the reaction pathway for UOR process: (a) Pathway 1 and 2. (b) Pathway 3.

concentration, aging time, and M^{2+}/M^{3+} molar ratios.[46] The hydrothermal method is the most common process and requires low cost to prepare LDH materials. This is a very realistic and easy procedure for the synthesis of LDHs by a hydrothermal way, in which a high-purity sample may be achieved. This process involves obtaining the precipitate by co-precipitation under high-pressure and high-temperature conditions in an autoclave. The high temperature and pressure help the growth of more well-ordered LDH layers. For $e.g.$, Kundu $et\ al.$ prepared NiCo-LDH over a Ni foam by mixing 0.146 g $Ni(NO_3)_2 \cdot 6H_2O$, 0.073 g $Co(NO_3)_2 \cdot 6H_2O$, and 0.13 g of urea in 35 mL of water to get a clear solution.[47] The solution and NF were transferred to an autoclave and heated to 180 °C for 12 h. Then the autoclave was cooled to room temperature and the synthesized NiCo-LDH over a Ni foam was cleaned with distilled water and ethanol, followed by drying at 60 °C for 12 h.[47] The sol–gel method is known for its fast and low-cost synthesis of nanoparticles with high purity, and high homogeneity with large surface area. This method allows a useful approach that enables precise control over the structure and composition of LDHs at the molecular level by adjusting the amount of reactant and aging time via adding or removing the reactant species. Prince $et\ al.$ proposed a sol–gel technique for the preparation of LDHs that can be tuned to acquire materials with the characterized morphology and specific metallic cations with very narrow pore size distributions around 3–4 nm and high specific surface areas up to 290 m^2 g^{-1}.[48] The microwave process is an energy-efficient, rapid route for synthesizing LDHs with high crystallinity-controlled morphology where aging occurs by microwave. Microwave Irradiation helps to increase the speed of the aging process by around 15–60 min. The particle with homogeneous size can be easily prepared by microwave techniques and the particle size is smaller than the particle prepared by reflux maturation. Bergada $et\ al.$ synthesized the MgAl-LDH by the combination of $Al(OH)_3$ and $Mg(OH)_2$ with the proportion of 1 : 4 molar ratio.[49]

5. Strategies for developing catalysts based on LDHs

Over the past few decades, LDH materials have attracted considerable attention, towards electrocatalytic UOR in the generation of H_2. However, the UOR remains thermodynamically and kinetically sluggish due to its complex six-electron transfer process, which involves both the adsorption of urea molecules and the desorption of N_2 and CO_2 molecules. Hence, it typically exhibits a high cell voltage in practical applications and limits the overall efficiency of the reaction. To address these significant limitations, various strategies have been employed in the pursuit of designing highly efficient urea oxidation catalysts.[3,38,50] These approaches aim to substantially enhance the catalytic activity and overall performance, thereby improving the efficiency of the UOR. Some of the strategies can be broadly categorized and discussed below.

5.1. Increasing catalytic active sites

Ni, Co and Fe-based LDH electrocatalysts have gained considerable interest as promising candidates for urea-assisted electrocatalytic H_2 production. These catalysts primarily serve as precursors that undergo self-oxidation to form the corresponding oxyhydroxides, widely considered as true active sites for the UOR.[24,51] However, this self-oxidation process requires extra energy during electrocatalysis and often leads to the dissolution of active metal sites during surface reconstruction, eventually decreasing the long-term stability of the catalyst. To mitigate these effects, the electronic structure of metals has been modulated through the introduction of a strong anchoring effect. This approach stabilizes the active sites, reduces energy requirements for self-oxidation, and enhances the overall durability of the catalyst during the urea oxidation process.

Several strategies have been used to successfully enhance the number of catalytic active sites. First, by introducing structural changes to the LDH framework, such as the generation of vacancies or the partial substitution of metal cations increases the surface area and facilitates the catalytic reactions. Further the density of active sites can be increased by employing metal doping with noble or non-noble metals (such as Ru, Au, Ag, and Ir) to encourage the formation of single-atom structures or nanostructured sites, which are very active for urea oxidation. Furthermore, the catalyst's electronic structure can be altered by the use of potent anchoring effects or interstitial anions, the newly formed active sites can be stabilized, the energy barriers for self-oxidation can be lowered, and the catalytic performance can be enhanced overall. These solutions result in more effective urea oxidation and improved stability, ensuring long-term durability and increased catalytic site density for the urea-assisted hydrogen generation process.

For example, cobalt-based LDHs have been demonstrated by Wang $et\ al.$ where a simple hydrothermal technique was employed to grow Cr-doped CoFe-LDH (CoFeCr-LDH) nanosheets on a nickel foam (NF) substrate.[52] This method resulted in an impressively low potential of 1.305 V $vs.$ RHE for the UOR at a current density of 10 mA cm^{-2}. This outstanding performance of the CoFe-LDH in the UOR has been recognized by the electron-withdrawing properties of Cr ions. In addition to this, they have developed a complete electrolyzer that was assembled with CoFeCr-LDH nanosheets as the anode and a Pt–C cathode for H_2 generation. When urea was added, the cell voltage needed to achieve a current density of 10 mA cm^{-2} decreased from 1.467 V to 1.329 V $vs.$ RHE, allowing for efficient H_2 production with a standard 1.5 V battery. Moreover, the surface area of a catalyst plays a critical role in its catalytic activity, as it determines the number of active sites available for the reaction. In recent years, interest has grown in enhancing electrocatalytic performance by exploring various catalyst morphologies. Studies have focused on designing catalysts with tailored geometries at the micro and nano scale regime, such as 1D nanowires, 2D nanosheets and nanobelts, and 3D nanotubes, showing great promise towards electrocatalysis. Hence, Zhang and his coworkers followed a different strategy, where they enhanced the catalytic activity of NiFe-LDH by decorating the rose-like Cu-doped Ni_3S_2 nanoflowers over the NiFe-LDH surface.[53] Interestingly, Cu–Ni_3S_2@ NiFe LDH-200 catalyst shows low overpotential of 216 mV at the current density of 100 mA cm^{-2} and become a potential catalyst

for urea electrolysis. The Cu–Ni$_3$S$_2$@NiFe LDH-200 (+)//Cu-Ni$_3$S$_2$@NiFe LDH-100 (−) electrode couple requires just 1.413 V *vs.* RHE to reach 10 mA cm^{-2} for urea electrolysis and operates stably for over 20 h, marking it as one of the most efficient catalysts reported. This study offers new insights into improving transition metal sulfides with LDHs. In addition to this, Su and colleagues reported a significant enhancement in the UOR performance through the rational design of a heterostructured electrocatalyst, combining NiMn-LDH nanosheets with NiCo$_2$S$_4$ arrays.[54] This innovative catalyst, fabricated *via* facile hydrothermal steps, benefits from high-flux electron transfer pathways at the interface, abundant active sites, and a unique three-dimensional architecture, which increases the overall active site density. The resulting NiCo$_2$S$_4$@NiMn-LDH heterostructure, supported on NF, demonstrates a low potential of 1.37 V *vs.* RHE at 100 mA cm^{-2} and a Tafel slope of 43.8 mV dec^{-1}. Remarkably, it exhibits robust stability for over 25 h at a current density of 50 mA cm^{-2} with minimal activity loss. Density functional theory (DFT) calculations indicate that the interface engineering significantly improves the adsorption and activation of urea molecules, enhancing the overall UOR dynamics by facilitating the dissociation of CO(NH$_2$)$_2$* into CO* and NH* intermediates, thereby leading to superior electrocatalytic performance.

5.2. Enhancing intrinsic activity for UOR

Enhancing the intrinsic activity of electrocatalysts for the UOR is critical for increasing the efficiency and energy savings in urea-assisted H$_2$ generation. Several solutions have been explored to solve issues such as sluggish intermediate desorption and catalyst structural optimization.

5.2.1. Optimizing *COO desorption. As a result of self-oxidation of catalysts, strong interaction between COO* and the formed oxyhydroxide (MOOH) results in sluggish UOR kinetics. Strategic modification of the desorption energy of COO* intermediates at the active sites is another strategy to promote the UOR process. Concurrently, Chen and colleagues have created a very effective UOR electrocatalyst, (NiFeCo)S$_x$/FeOOH/NiFeCo(OH)$_x$, supported on a conductive NF.[55] This was achieved through the application of a straightforward, low-energy, single-step corrosion engineering technique. Excellent UOR performance is achieved by the heterostructure, which combines the high conductivity of (NiFeCo)S$_x$, abundant Fe^{3+} in amorphous FeOOH, and the catalytic activity of NiFeCo(OH)$_x$. Together with outstanding stability, the catalyst showed an ultra-low potential of 1.36 V *vs.* RHE at 100 mA cm^{-2} and a modest Tafel slope of 24.8 mV dec^{-1}. DFT simulations revealed that the formation of heterointerfaces optimizes the adsorption and desorption energies of the intermediate by regulating the d-band center. The downshift of the d-band center results in improved desorption ability of UOR intermediates during the process. Improving the desorption process is essential to increasing the material's total catalytic activity.

5.2.2. Developing synergistic and morphological enhancements. Tailoring the structural and electronic features of the catalyst can also increase the intrinsic activity. Feng *et al.*

created a CoNi-LDH/Fe MOF heterostructured electrocatalyst on an NF substrate, especially for the UOR process.[56] The UOR, which has a lower equilibrium potential than that of the OER, drastically reduces the overpotential at the same current density, making the overall process more energy efficient. They have also designed a two-electrode system (Pt/C/NF||CoNi-LDH/Fe MOF/NF), where the inclusion of the UOR lowers the cell voltages (1.34, 1.45, and 1.55 V) by 30 to 60 mV compared to the OER, significantly reducing energy consumption for H$_2$ production. This highlights UOR's potential in achieving efficient H$_2$ generation with minimal energy input. Kim *et al.* demonstrated the synthesis of amorphous, porous 2D NiFeCo hydroxide nanosheets on NF by a simple, cost-effective electrodeposition method.[57] This material exhibited remarkable bifunctional electrocatalytic activity for both alkaline water splitting and urea electrolysis, showcasing its intrinsic catalytic efficiency. The outstanding performance was largely attributed to the amorphous structure, 2D nanosheet morphology, and the synergistic effects of Ni, Fe, and Co, which significantly enhanced the material's active sites and conductivity. For the UOR, the electrode demonstrated a low potential of 0.280 V (*vs.* SCE) at 10 mA cm^{-2} in a 1 M KOH solution with 0.33 M urea. The urea-based water electrolysis cell operated with just 1.49 V *vs.* RHE to achieve 10 mA cm^{-2}, with excellent stability. This study highlights the superior intrinsic activity of the NiFeCo LDH/NF material and its potential for robust, earth-abundant electrocatalysts in sustainable water splitting and urea oxidation applications.

5.2.3. Doping and pre-oxidation. Zhang and colleagues developed NiCoV-LDH nanosheet arrays on a NF substrate by a strategy of V-doping coupled with H$_2$O$_2$ pre-oxidation by a hydrothermal method.[58] The NiCoV$_{1.0}$-LDH/NF-100 composite exhibited the highest UOR and HER activities due to its increased active sites. The optimal nanosheet structure was subsequently grown *in situ* on reduced graphene oxide (rGO) to form the NiCoV$_{1.0}$-LDH/rGO/NF-100 composite, achieving a low potential of 1.33 V *vs.* RHE for the UOR and an overpotential of 70 mV for the HER at 10 mA cm^{-2}. Furthermore, the composite required only 1.45 V for urea-assisted water electrolysis, outperforming many non-precious metal catalysts. Further, in the *in situ* Raman spectra, characteristic peaks were observed at 465 and 527 cm^{-1}, indicating Ni^{2+}–O vibrations in NiCoV$_{1.0}$-LDH/NF-100. Moreover, the surface reconstruction of the catalyst occurred, evidenced by a new peak at ∼550 cm^{-1}, attributed to Ni^{3+}–O (NiOOH) vibrations, when the potential was increased to 1.40 V. Concurrently, the peak at 810 cm^{-1}, corresponding to the stretching vibration of V–O bonds, which gradually diminished with the increase in potential, suggested the gradual consumption of V. The same surface reconstruction was observed at a lower potential (1.3 V) in the presence of the UOR, suggesting that the presence of urea facilitated this process at a lower overpotential. Furthermore, the peak at 1003 cm^{-1}, attributed to the N–C–N symmetrical vibration of urea, gradually decreased with the increase in potential, indicating the gradual consumption of urea during the reaction. The V-doping and H$_2$O$_2$ pre-oxidation were shown to enhance the electronic

environment of Ni and Co sites, leading to more highly valent Ni^{3+} and Co^{3+} species, reduced adsorption energy of urea, and improved water dissociation. This study demonstrates that V-doping represents a promising strategy for optimizing the UOR performance in urea-assisted water electrolysis technologies.

The intrinsic activity of UOR electrocatalysts has been greatly enhanced by combining these strategy, namely modulating desorption energies, optimizing structural and electronic properties, and using sophisticated doping techniques, making it possible to produce H_2 in an efficient, long-lasting, and energy-efficient manner.

6. Application of LDHs and their derivatives as electrocatalysts for the UOR

In recent times, numerous electrocatalysts have been developed for urea electrolysis (urea-coupled water electrolysis), an alternative to the conventional OER process of water electrolysis. This process exhibits a lesser theoretical potential (0.37 V vs. RHE) than the water-splitting process (1.23 V vs. RHE) for the generation of H_2. Recent studies reported in the literature recommend that LDH-based materials are emerging and potential candidates for the UOR process. This review provides a comprehensive understanding of recent trends and efforts on LDH-based electrocatalysts for the UOR. We briefly covered the existing strategies on LDHs and their derivatives as electrocatalysts for UORs, such as pristine LDHs, doping, defect/intercalation and more importantly heterostructure with different chalcogenides and oxide moieties. Finally, we proposed the perspectives on potential directions for future studies on LDH-based materials towards urea electrolysis.

6.1. Pristine LDHs

The metals with a higher oxidation state can easily tune the electronic properties of other metals, resulting in an enhanced performance. For example, Ni-based catalysts are very promising candidates for the UOR process, due to the spontaneous oxidation of Ni species (Ni^{3+}), which serves as an active site for the reaction.[59,60] For instance, Zhang and his colleagues tuned the oxidation state of Ni by high-valent Mn and prepared ultrathin NiMn-LDH (U-NiMn-LDH/CFC) nanosheets directly on a CFC (carbon fiber cloth) matrix via a simple hydrothermal approach.[61] The in situ growth of electrocatalysts on a three-dimensional-structured substrate results in high conductivity (including CFC, NF, and Ti mesh), which further simplified the fabrication procedures and improved the mechanical stability of the electrode compared to powder-coated matrix electrodes. Moreover, the nanoarray structure exhibited improved catalytic activity by providing abundant active sites, facilitating the movement of electrolytes and promoting the diffusion of reaction products. The U-NiMn-LDH nanosheet array was highly favorable for exposing catalytic active sites, in contrast to bulk NiMn-LDH (B-NiMn-LDH), delivering remarkable electrocatalytic performance towards the OER, UOR, and HER. In this study, the presence of Mn in the U-NiMn-

LDH/CFC nanosheet revealed that the oxidation of Ni^{2+} to Ni^{3+} appeared at a lower potential than that of $Ni(OH)_2$/CFC, demonstrating the enhanced capacity of Ni^{2+} to Ni^{3+} and thus improving the electrocatalytic activity of U-NiMn-LDH/CFC. Particularly, it showed high performance towards UOR (0.5 M urea + 1 M KOH) with 1.351 V vs. RHE at 20 mA cm^{-2} and 169 mV at 10 mA cm^{-2} for HER. This enhanced activity is due to the ultrathin nanosheet structure of NiMn-LDH, which provides more accessible active sites. Moreover, the 3D network of substrate further improves the conductivity, which results in higher activity towards UORs. Later, Li et al. investigated the behavior of a common catalyst, NiFe-layered double hydroxide (NiFe-LDH), during the urea oxidation reaction (UOR) in an alkaline solution.[62] They demonstrated that Fe^{3+} and slightly changed $Ni^{2+\delta}$ ions serve as the active sites for the UOR, both before and after Ni oxidation. Operando Raman spectroscopy suggests that in NiFe-LDH, a peak above 0.5 V vs. RHE represents the formation of $Ni(OH)_5O^-$ intermediates during the UOR process. At a potential below 0.5 V, protons and electrons from urea are captured by Fe^{3+} sites, as evidenced by the observed Fe^{3+}–OOH vibration peak before the NiOOH peak. Following the phase transition (via Argon plasma treatment), the Fe^{3+}–OOH vibration peak disappears, suggesting the transfer of adsorbed OH^- from Fe to Ni sites and the formation of $Ni^{2+\delta}O_xH_y$ as the active center in the higher potential region. Further, the operando electrochemical impedance analysis (EIS) in the low-potential region (0.3–0.5 V) indicated that the electrolyte resistance (R_s) is independent of urea concentration. Moreover, the observed slight decrease in the intermediate phase angle evident from a Bode plot during both the OER and the UOR on NiFe-LDH at low potentials, concluding that the OER originates due to the accumulation of intermediates, whereas the UOR involves a direct electron transfer mechanism related to adsorbed oxygen on the Fe sites. The UOR-coupled H_2 generation device requires lower cell voltages than those of the conventional overall water-splitting device, operating at 1.72 V and 1.892 V vs. RHE for 100 mA cm^{-2} and 300 mA cm^{-2}, respectively. This signifies a reduction of 76 mV and 90 mV, respectively. In conclusion, the UOR occurs on NiFe-LDHs before the OER, and by utilizing various active sites, the reaction can occur on both the pristine NiFe-LDH and the derivative $Ni^{2+\delta}O_xH_y$ phase. The $Ni^{2+\delta}O_xH_y$ derivative's robust oxidising activity and capacity to regenerate the active site catalyze the UOR in the high-potential region. As a result, the reaction kinetics is boosted and simultaneously leads to the occurrence of OER and UOR processes.[62] Despite the high performance of pristine LDHs, it suffers from several drawbacks such as low electrical conductivity, limited active site and poor stability. For the activity and performance of pristine LDHs, various strategies can be employed, including increasing layer charge density, surface functionalization by defect creation, intercalation of functional organic molecules, hybridization or creating heterostructures with other materials, doping with noble/non noble metals or nanoparticles, and substitution with cations or anions. These modifications can effectively optimize the performance of LDH-based materials for a wide range of applications. Each method can be tailored depending on the specific functional requirements of the material and some of them are briefly discussed in this review.
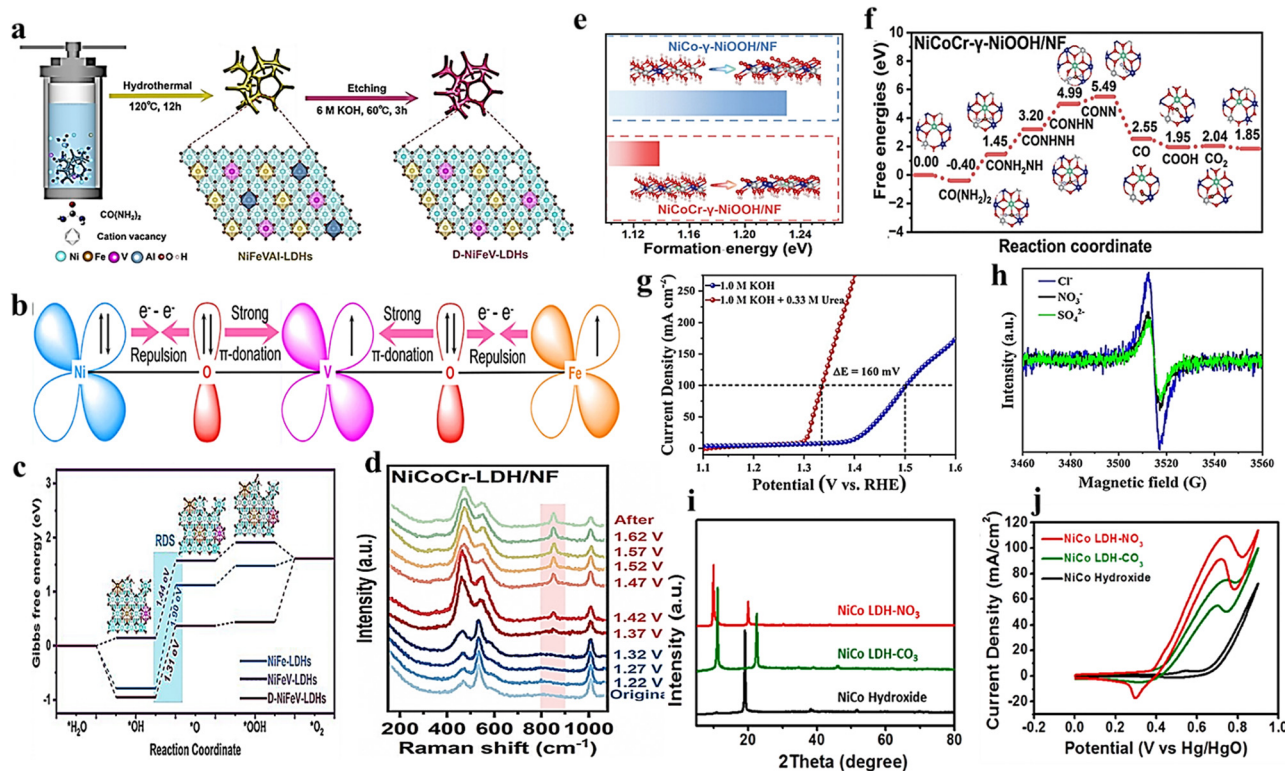
Fig. 3 (a) Schematic of the preparation process of D-NiFeV-LDHs over NF. (b) Schematic of the electronic coupling between Ni, Fe, and V atoms within the D-NiFeV-LDH structure. (c) Gibbs free energy values for OER intermediates on NiFe-LDHs, NiFeV-LDHs, and D-NiFeV-LDHs. Reproduced from ref. 60 with permission from Elsevier. (d) In situ Raman spectra of NiCoCr-LDH/NF during the UOR. (e) Formation energy of γ-NiOOH in NiCoCr-γ-NiOOH/NF and NiCo-γ-NiOOH/NF. (f) Gibbs free energy profiles for the UOR pathway on NiCo-γ-NiOOH/NF and NiCoCr-γ-NiOOH/NF. Reproduced from ref. 66 with permission from Wiley-VCH. (g) LSV polarization outcomes of O_V-NiFe-LDH in 1 M KOH solution with and without 0.33 m urea. (h) EPR spectra of O 1s in O_V-NiFe-LDH samples with different iron sources. Reproduced from ref. 67 with permission from Elsevier. (i) XRD pattern if NiCo-LDH and NO_3^-, CO_3^{2-}-intercalated NiCo-LDH. (j) LSV polarization results of NiCo-LDH, NiCo-LDH-NO_3^- and NiCo-LDH-CO_3^{2-}. Reproduced from ref. 27 with permission from the American Chemical Society.

6.2. Defects and intercalation

Defect refers to an imperfection or irregularity in the atomic or molecular structure of a material. Defects can have a significant impact on the properties of the material, including its electrical, thermal, mechanical, and chemical behavior. Bulk LDHs often exhibit limited specific surface area and poor conductivity, which significantly hinder their electrocatalytic performance.[61,63] Previous studies have shown that 2D nanomaterials with single or few atomic layers significantly enhance the surface area and active site exposure, leading to improved catalytic performance. Intercalating anions of different sizes can alter the interlayer distance. Further exfoliating bulk LDHs into ultrathin nanomaterials creates numerous edges, corner sites, and dangling bonds, which can serve as active sites with lower coordination. Intercalation/exfoliation into ultrathin 2D nanosheets can induce surface atoms to escape from the lattice, forming defects. This disordered structure lowers surface energy and enhances stability. Moreover, structural defects and disorder in ultrathin 2D nanosheets can alter the coordination number of active sites, affecting their electronic structure and ultimately influencing catalytic activity. In view of this, Li et al. synthesized a novel V-doping-defective NiFe-layered double hydroxide nanosheet (D-NiFeV-LDH) over the NF via a hydrothermal and alkali-etching strategy, as an efficient

electrocatalyst (Fig. 3a).[64] By precisely tuning the local coordination environments of the catalytically active sites through high-valence V-doping and introducing Fe^{3+} cation-vacancy defects, the material offers significantly more active sites. As a result, defect-rich D-NiFeV-LDHs demonstrate a remarkably low overpotential of 196 mV and a potential of 1.34 V vs. RHE at a current density of 10 mA cm^{-2}, towards the OER and UOR, respectively. The doping of V over the defective NiFe-LDH results in the aggregation of V in the host lattice with Ni and Fe through O^{2-} bridging (Ni–O–V–O–Fe), as displayed in Fig. 3b. The electron-rich t_{2g} of Ni^{2+} and Fe^{3+} transfer electrons to the deficient t_{2g} d-orbitals of V^{5+} and V^{4+}, leading to enhanced delocalization of π-symmetry electrons among the Ni, V, and Fe atoms within the LDH structure. As illustrated in Gibbs's free energy diagram (Fig. 3c), the delocalization of electrons between Ni–O–V–O–Fe bonds facilitates moderate adsorption and desorption of OER and UOR intermediates. In addition, the conductivity can be increased by the in situ growth of LDH materials over the conductive substrates. Moreover, it provides enhanced active surface area, increased exposure of edge catalytic sites, facilitated release of gaseous products, and improved mechanical strength. For instance, Chen et al. proposed an in situ-grown high-performance 2D NiFe-LDH/NF (H-NiFe LDH) nanosheet arrays with many holes on the surface as

electrocatalysts for urea-rich industrial water splitting.[65] The presence of a PEO–PPO–PEO (P_{123}) block copolymer as a soft template induces holes on the surface. The presence and subsequent removal of P_{123} in NiFe-LDH nanosheets result in the formation of holes, leading to a defective or disordered structure. This, in turn, increases the exposure of edge catalytic sites and expands the active surface area. As a result, HER performance increased with 189 mV as overpotential, which is lower than that of NiFe LDH/NF (204 mV) in 1 M KOH with 0.33 M urea and showed 1.48 V *vs.* RHE to reach 100 mA cm^{-2} current density towards the UOR. Further, it demands a very less cell voltage of 1.418 V *vs.* RHE for H-NiFe-LDH/NF||H-NiFe-LDH/NF to reach 10 mA cm^{-2} current density with 25 h stability towards total water splitting. The high performance of NiFe-LDHs is solidly due to NiFe-LDH nanosheets on the NF offering enhanced surface area and active sites, facilitating the HER, OER, and UOR. The inductive effect of P_{123} creates oxygen vacancies (O_v), improving charge transfer. The interconnected nanosheet arrays provide channels for efficient mass and charge transfer, leading to superior overall performance. Another type of defect is the formation of an O_v, which modifies the LDH's electrical structure, provides free electrons which will increase the electronic conductivity and boosts the electrocatalytic performance. Xu *et al.* demonstrated that the incorporation of Cr into the NiCo-LDH significantly enhances the performance of UOR *via* the creation of O_v and an LDH lattice with abundant defects with a low potential of 1.38 V at 100 mA cm^{-2} current density with 45 h long-term stability.[66] *In situ* structural and Raman studies revealed that Cr doping effectively modifies the electronic state and defect-rich coordination environment of NiCo-LDHs with the formation of active intermediate γ-NiOOH (Fig. 3d). DFT studies disclose that the incorporation of Cr fastens the electron transfer of NiCoCr-γ-NiOOH/NF to adsorb urea molecules with a charge density difference of 0.28 e$^-$. Further, a reduced O–H bond interaction caused by a shorter hybridization energy range between O-2p_z and H-1s orbitals results in a lower formation energy of γ-NiOOH (Fig. 3e). Hence, the addition of Cr increased the urea molecules adsorption and their intermediate adsorption energy and enhanced the UOR performance (Fig. 3f). With its excellent electrocatalytic performance, unique electronic states, and coordination structures, the NiCoCr-LDH/NF electrode demonstrated great potential for practical applications in energy catalysis. Similarly, Liu *et al.* created abundant O_v in NiFe-LDHs by etching the bare NF with Fe^{3+} and Cl$^-$ ions *via* a redox reaction, resulting in the formation of NiFeCl(OH)$_x$ on the NF surface.[67] The removal of Cl$^-$ ions creates O_v in the NiFe-LDH nanolayers, as confirmed by the electron paramagnetic resonance (EPR) and X-ray photoelectron spectroscopy (XPS) analyses. Further, with different Fe-containing anions (Cl$^-$ (49.2%) surpassed NO$_3^-$ (39.5%) and SO$_4^{2-}$ (39.2%)), the proportion of O_v was increased, as shown in Fig. 3h, suggesting that Cl$^-$ etching has more tendency to create more O_v *via* replacing OH$^-$ and subsequent volatilization of Cl$_2$ atoms. Electrochemical assessments indicate that O_v enhanced electrical conductivity and boosted surface area, resulting in a 4.1-fold enhancement in electron transport and a 5.1-fold increase in active catalytic sites. In addition, they observed that with the increase in the concentration of Fe^{3+}, the morphology of the LDH varied with the reduction in layered thickness. The O_v-NiFe-LDH exhibits excellent performance of 1.30 V *vs.* RHE to meet a current density of 10 mA cm^{-2} with a difference of 160 mV from the conventional OER (Fig. 3g). Further, DFT analysis also demonstrates that the introduction of O_v lowered the free energy required for urea chemisorption and strengthened the bond with the *CONHNH intermediate, which significantly improving the UOR. Another modification strategy involves intercalating anions of different sizes to alter the 2D LDH interlayer distance, affecting the electrocatalytic surface area and performance. Additionally, anion replacement can modify the surface-active sites, potentially improving the metal-hydroxyl bonding and enhancing the catalytic activity. Zeng *et al.* studied the effect of intercalating different-sized anions such as NO$_3^-$ and CO$_3^{2-}$ ions over the NiCo-LDH towards the UOR.[27] The NiCo-LDH with NO$_3^-$ intercalated disclosed a higher activity with an onset of 0.37 V *vs.* Hg/HgO and stability towards the UOR than the CO$_3^{2-}$ intercalated ions. The high performance of NiCo-LDH NO$_3^-$ is attributed to increased interlayer spacing (0.86 nm) and reduced crystallite size ($\sim$13.4 nm) as a result of the intercalation of NO$_3^-$. Moreover, the XRD patterns demonstrate the lattice expansion of the ordered brucite NiCo-LDH structure along the z-axis after the intercalation of NO$_3^-$ and Co$_3^{2-}$ ions (Fig. 3i). The cyclic voltammograms of intercalated and bare NiCo-LDH showed distinct electrochemical behavior, which suggested that during backward scan, the current density of the peak is lower than that of the forward scan (Fig. 3j). This lower peak current density indicates ineffective desorption of urea products during the course of the UOR process. Further, the effect of urea concentration suggests that with the increase in concentration from 0.1, 0.2 to 0.33 M, the NiCo-LDH displayed characteristic oxidation peaks in both forward and backward scans with a noticeable increase in current. However, a further increase in concentration beyond 0.5 M resulted in only a slight current increase, suggesting the depletion of urea molecules near the electrode. It is evident that the UOR at lower and higher concentrations is a kinetically and diffusion-controlled process respectively.[27] In another work by Hong *et al.* Au^0, Ag^0 and Pd^0 noble metal nanoparticles were intercalated over the 3D hierarchical NiCo-LDH as an efficient electrocatalyst for the UOR.[68] The decorated LDH showed a UOR activity of Au/NiCo-LDH > Pd/NiCo-LDH > Ag/NiCo-LDH. The higher activity of Au over NiCo-LDH is owing to the 3D network-like porous structure of the interconnected nanosheets (NSAs) by increasing its surface-to-volume ratio and exposing a larger number of active sites. Moreover, the open channels within the nanosheets facilitate strong interaction between the reactants and the catalyst and also ensure the efficient removal of gaseous byproducts. In other words, the presence of Co ions would help to form a NiOOH phase at a very lower potential. Moreover, the decorated/intercalated Au further improves the formation of Ni^{3+} ions (active site) by reducing the energy barrier, thereby enhancing urea adsorption on the catalyst surface and promoting the overall reaction kinetics. Furthermore, Au improves the electron-conducting pathways (improves electrical conductivity) due to their strong interaction with the LDH substrate.

In summary, introducing additional cations or anions into the brucite LDH structure effectively modifies its specific physical and chemical properties. These modifications can effectively enhance the active site for oxidation reactions, leading to improved performance and stability with high selectivity.

6.3. Elemental doping

The flexibility of LDH composition allows for the doping or incorporation of various earth-abundant elements, which can offer unique catalytic properties when strategically engineered within the LDH structure. Doping LDHs with a third metal can effectively modify their morphology, electronic structure, and electrical conductivity, leading to enhanced electrocatalytic performance. Moreover, the synergistic interactions between dopants and active sites will optimize the adsorption/desorption energies of intermediates, facilitating electron transfer kinetics and boosting the intrinsic catalytic activity for oxidation reactions.[69,70]

Doping techniques are turned to be specific for definite doping elements such as metal doping, non-metal doping, or the simultaneous incorporation of multiple elements[71,72] For instance, Liu *et al.* engineered a NiFe-LDH with redox-inactive Cu using the sol–gel method to potentially enhance the electronic properties of Ni, which has lower Lewis acidity compared to Cu.[25] As a result, a Cu-doped NiFe LDH displays a low overpotential of 123 mV at 100 mA cm^{-2} and a stability of 300 h at 10 mA cm^{-2} current density in 1 M with 0.33 M urea (Fig. 4a and b), compared to the conventional OER process. The XANES results implied that the incorporation of Cu towards NiFe-LDHs effectively tunes the oxidation state of +2 to the average oxidation state of 2.92 (NiOOH), which will be highly active towards UORs without undergoing self-oxidation during the process (Fig. 4c). Moreover, the overall urea-assisted water splitting demands very low overpotential of 100 mV to reach 10 mA cm^{-2} with 100 h long-term stability. Recently, with a similar strategy, Yu and his group
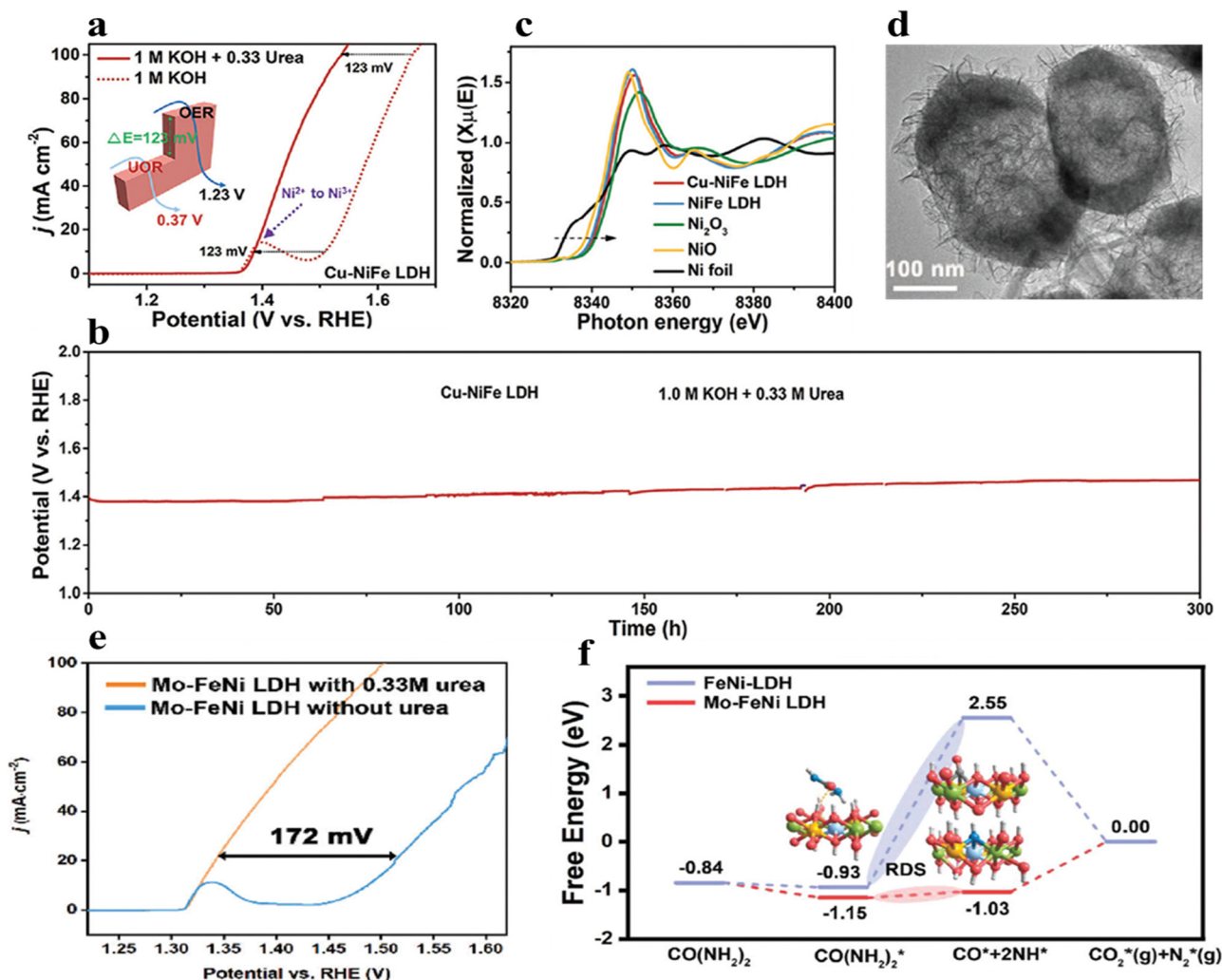

Fig. 4 (a) LSV polarization results of Cu NiFe-LDH with and without urea in 1 M KOH solution. (b) Chronopotentiometric curves showing stable performance up to 300 h under UOR conditions. (c) Ni K-edge XANES spectra of Cu NiFe-LDH, indicating that the doping of Cu increases the valence state of Ni. Reproduced from ref. 21 with permission from Wiley-VCH. (d) TEM images showing the distinct spindle-like hollow structure of Mo-FeNi LDH. (e) LSV polarization outcomes of Mo-FeNi LDH in 1 M KOH solution with and without 0.33 m urea. (f) Gibbs free energy diagrams for the three steps of the UOR for Mo-FeNi LDH and FeNi-LDH. Reproduced from ref. 22 with permission from Wiley-VCH.

members engineered high-valence-state NiOOH in FeNi-LDHs, derived from spindle-like Fe-MIL-88A by doping high-valence metal ions such as Mo, Mn, and V for a better UOR process.[26] As evident from Fig. 4d, further doping of high-valence Mo resulted in ultrathin nanosheets over the outer layer of the FeNi-LDH with the retention of the spindle-like morphology of Fe-MIL-88A. Further, the introduction of high-valence metal ions resulted in an expanded FeNi-LDH lattice due to their larger atomic radii. The combination of lattice expansion, optimized electronic structure, and hollow structure in optimized Mo-FeNi LDHs exhibits exceptional activity with a potential of 1.32 V *vs.* RHE at 10 mA cm^{-2} (Fig. 4e) and durability for 12 h at 50 mA cm^{-2} under the UOR condition in alkaline solutions. The increased performance of Mo-FeNi LDHs is attributed to a decrease in the free energy associated with various intermediates of the UOR, as evidenced by the free energy analysis demonstrated in Fig. 4f. In addition, several NiFe-LDH-based electrocatalysts were reported. For example, Wang and his group members have explored Rh doping over the NiFe-LDH with 1 M KOH + 0.33 M urea as the electrolyte.[73] The Rh-doped NiFe-LDH disclosed a significant improvement in performance of 9.8 times compared to the conventional OER analysis. Very recently, Cao *et al.* developed a NiFe-LDH doped with high-valent Hf^{4+} over an NF as the efficient electrocatalyst for the UOR (1 M KOH + 0.5 M urea).[69] It is observed that doping of Hf regulates the adsorption of UOR intermediates by modulating Ni^{2+} to a higher valence state, resulting in very low potential of 1.37 V *vs.* RHE to attain 100 mA cm^{-2} current density. Furthermore, Wu and colleagues employed *in situ* Raman spectroscopy to investigate the formation of higher-valent NiOOH species within Mn-doped NiMn-LDHs.[70] *In situ* Raman spectroscopy reveals that doping of Mn promotes the formation of high-valence Ni^{3+}OOH in NiMn-LDHs. This enhancement in the oxidation state of Ni^{2+} to Ni^{3+} contributes to a reduction in the onset potential from 0.4 V to 0.3 V *vs.* Hg/HgO compared to the undoped NiMn-LDH towards UOR. In addition to the transition of oxidation state, Raman spectroscopy analysis indicates that Mn doping in NiMn-LDHs results in elongated Ni–O bonds within the NiOOH structure and increased phase disorder under UOR potentials. In addition to cation doping, Wang *et al.* successfully created a partially amorphous fluorine-modified nickel-iron layered double hydroxide (NiFe-F) using a low-temperature fluorination process with hydrofluoric acid (HF) *via* a one-step hydrothermal process.[74] The incorporation of F with the amorphous regions generates numerous O$_v$, creating a material with abundant active sites for electrocatalytic reactions. The modified NiFe-F-4 material demonstrated exceptional UOR performance, requiring remarkably a low potential of 1.44 V *vs.* RHE to achieve a current density of 50 mA cm^{-2}. In summary, the doping of LDH-based electrocatalysts is a powerful strategy to enhance their performance. This strategy tunes the morphology of LDH, increases the surface area and electrical conductivity, and also introduces new active sites. Especially, doping of higher valence metal ions can effectively tune the electronic structure and enhance the intrinsic catalytic activity of LDHs. These combined effects contribute

to an improved UOR process than the conventional OER and other electrocatalytic applications.

6.4. Heterostructures and derivatives of LDHs

LDHs are well known for their exceptional catalytic capabilities, primarily attributed to their greater number of active sites and distinctive electronic structure. Unfortunately, the active sites exposed by traditionally synthesized LDHs, often characterized by thick, irregular formations, are notably restricted and inherently less reactive. To overcome these issues, creating a heterojunction with other materials having a difference in work function will effectively regulate the electronic structure, leading to a redistribution of charge and a significant boost in electrocatalytic activity.[55,75–80] It is important to note that such a heterostructure, formed by combining two materials with different work functions, naturally produces a built-in electric field. This field can facilitate the transfer of charge and promote charge redistribution. For instance, Wang *et al.* created a NiFe-LDH heterostructure (Fig. 5a) with N-doped carbon-supported Co (Co-NC@NiFe LDH) as a superior electrocatalyst for the UOR and OER in an alkaline medium.[81] The heterostructured Co-NC@NiFe LDH requires an overpotential of 200 mV to achieve a current density of 10 mA cm^{-2} during the OER. However, for the UOR, a much lower potential of 1.36 V is required to reach a current density of 100 mA cm^{-2}. The density of states (DOS) displayed in Fig. 5b show that the formation of heterostructures significantly alters the molecular orbitals and regulates the energy gap between the highest occupied molecular orbital (HOMO) and the lowest unoccupied molecular orbital (LUMO). While the NiFe-LDH shows a HOMO–LUMO gap of 0.74 eV, the Co-NC@NiFe LDH exhibits a negligible energy gap, suggesting efficient electron transfer. Interestingly, the DOS of the Co-NC@NiFe LDH primarily arises from Co, Ni, Fe, and O rather than C and N, indicating that the adsorption of both the catalysts and the reaction intermediates depends on the electronic interactions between these elements. Moreover, the electronic interaction at the interface can influence the d-band center, affecting the adsorption of reaction intermediates (Fig. 5c). The d-band center positions of Co-NC, NiFe LDH, and Co-NC@NiFe LDH were found to be -1.18, -1.1, and -1.05 eV, respectively. The higher d-band center of the Co-NC@NiFe LDH suggests fewer antibonding states with the reaction intermediates and stronger bonding with oxygen, contributing to its improved OER activity. The same might be the reason for the improved UOR performance.[81] Despite the advantages of LDHs, it faces limitations in terms of electrical conductivity and stability, which could be encountered by combining crystalline and amorphous components. Ci *et al.* developed a novel approach by combining amorphous nickel-iron hydroxide nanosheets with crystalline nickel molybdenum oxide *via* electrodeposition.[82] This hybrid material demonstrated exceptional performance as an electrocatalyst for both the OER and UOR with overpotential of 233 mV (at 10 mA cm^{-2}) and 1.45 V (at 100 mA cm^{-2}), respectively. Moreover, the hybrid acid/base urea electrolytic system (NiFe-LDH/NiMoO$_4$/NF|Pt/C/NF) exhibited an impressive performance, requiring only 0.59 V *vs.* RHE to achieve a current density of
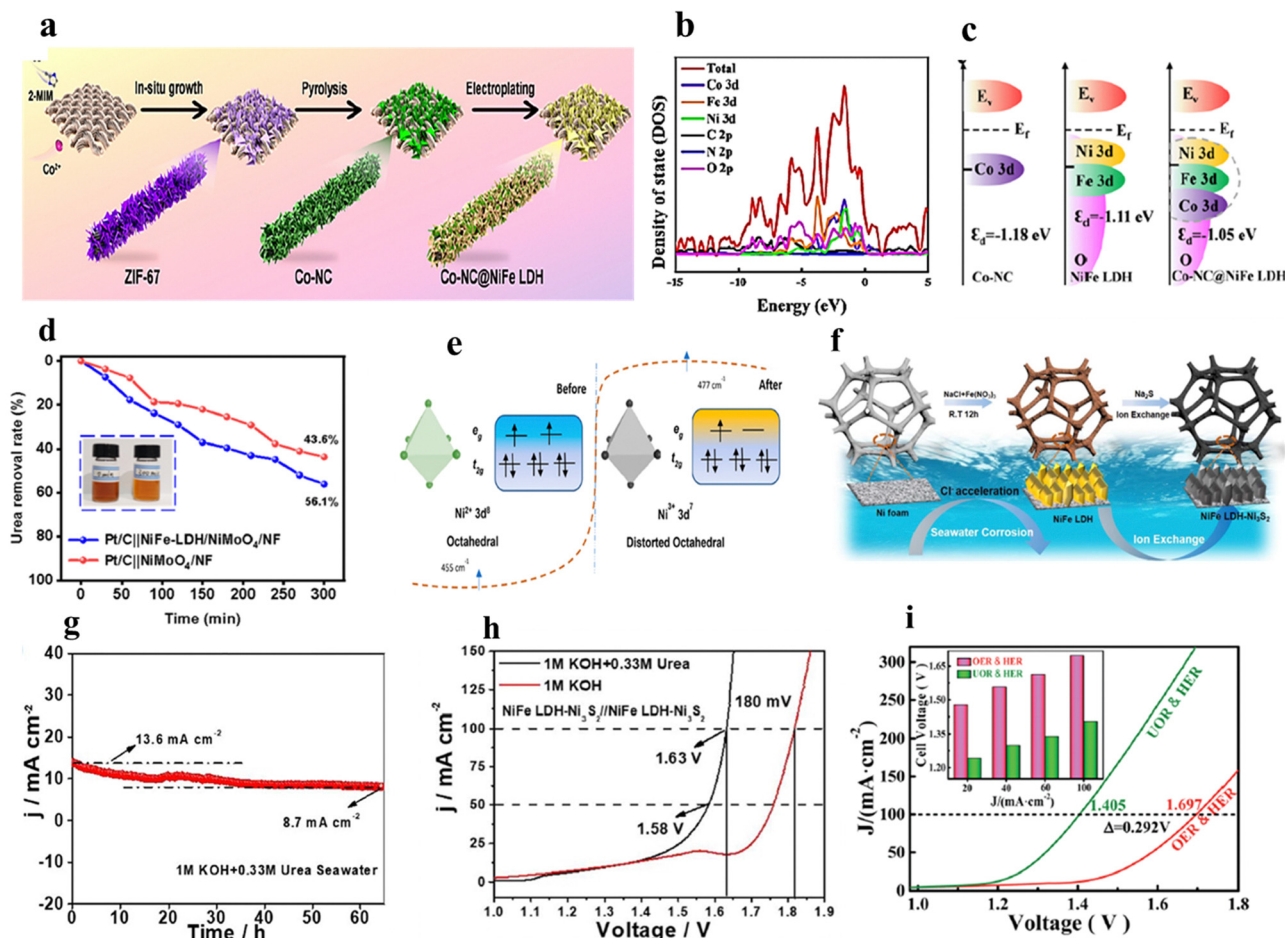
Fig. 5 (a) Schematic of the synthesis of Co-NC@NiFe LDH. (b) and (c) Density of states and d-band center of Co-NC@NiFe LDH. Reproduced from ref. 80 with permission from the Royal Society of Chemistry. (d) Urea degradation ability of the Pt/C||NiFe-LDH/NiMoO$_4$/NF electrolyzer (inset: color change of electrolyte before and after electrolysis). Reproduced from ref. 81 with permission from Wiley-VCH. (e) Electronic configuration of Ni^{2+} and Ni^{3+} in NiFe-LDH@NH$_2$-G before and after the stability test towards the OER process. Reproduced from ref. 84 with permission from the American Chemical Society. (f) Schematic of the synthesis of a 3D desert rose flower-shaped hierarchical NiFe LDH-Ni$_3$S$_2$ catalyst *via* seawater corrosion. (g) LSV results demonstrating the overall water splitting performance of NiFe LDH-Ni$_3$S$_2$ without and with 0.33 M urea in 1 M KOH. (h) Corresponding long-term stability in 0.33 M urea in 1 M KOH. Reproduced from ref. 85 with permission from the Royal Society of Chemistry. (i) Polarization outcomes of the MoP@NiCo-LDH/NF-20||MoP@NiCo-LDH/NF-20 in 1 M KOH with or without 0.5 M urea (inset: comparison of driving voltages for urea and water electrolysis at various current densities). Reproduced from ref. 86 with permission from the Royal Society of Chemistry.

10 mA cm^{-2}. Additionally, it demonstrated remarkable long-term stability, operating for 80 h at a current density of 120 mA cm^{-2} without significant degradation. Further, the concentration study on urea in the electrolytic cell demonstrates, after 300 min of electrolysis, that NiFe-LDH/NiMoO$_4$/NF degraded 55.6% of the urea, which was higher than the 43.6% degradation rate observed in the NiMoO$_4$/NF in the electrolyte (Fig. 5d). These observations indicate that NiFe-LDH/NiMoO$_4$/NF not only generates H$_2$ but also acts as a sacrificial anode and degrades the urea in the urea-rich wastewater. Further, the metal/semiconductor-contact-induced Mott–Schottky heterojunction can facilitate spontaneous electron transfer across the interface, leading to the exposure of additional active sites. This concept presents a promising strategy for the deliberate design of heterostructured catalysts. For example, Zaho *et al.* created a three-phase Mott–Schottky heterojunction by employing a two-step hydrothermal process and subsequent spontaneous reduction of Ag ions

over the NiFe-LDH, resulting in the formation of NiFe-LDH/NiFe$_2$O$_4$.[83] The close proximity of Ag over the NiFe-LDH achieved through *in situ* growth and combined with the electron redistribution facilitated by the Mott–Schottky heterojunction at the interface results in remarkable catalytic performance for both the OER and the UOR. The heterostructure requires a low overpotential of only 249 mV to achieve a current density of 100 mA cm^{-2} and a low Tafel slope of 42.79 mV dec^{-1} towards the OER, indicating efficient electron transfer through the heterojunction. Additionally, it can drive the UOR at a potential of 1.389 V *vs.* RHE to reach a current density of 50 mA cm^{-2}, demonstrating its potential for promoting urea oxidation. Further, *in situ* Raman spectroscopy analysis explained that the addition of Ag to the heterostructure results in the formation of high-valence Fe and Ni species before the onset of the OER (at a lower applied potential of 1.1 V), resulting in a large number of active sites and simultaneously improving the

performance. Besides, Su and his co-workers tuned the Fermi energy level by constructing a p–n heterojunction and a strong built-in electric field between NiP nanorods (p-type) and amorphous NiFe-LDHs (n-type) over the NF.[84] This p–n junction facilitates the OH$^-$ adsorption and enhances the cleavage of chemical bond of urea by establishing oppositely charged regions at the interface. Moreover, upon incorporating Mo into NiP, a strong built-in electric field was achieved. This strong built-in electric field (*i.e.* electron redistribution) at the heterostructure between the NiMoP/NiFe-LDH exhibited superior OER and UOR activities, achieving ultralow overpotentials of 237 mV and 120 mV at 100 mA cm^{-2}, respectively. After the formation of a p–n heterojunction, a spontaneous hole-charge region with a built-in potential of 1.2 V compared to NiP/LDH (1.0 V) is formed at the p–n junction interface between NiMoP (NiP) and NiFe-LDHs. As a result, electrons are transferred from the n-type NiFe-LDH to the p-type NiMoP (NiP). This leads to a higher concentration of negatively charged active sites on the NiMoP side and positively charged active sites on the NiFe-LDH side. Hence, the electrostatic interactions within the p–n junction facilitate the adsorption of OH$^-$ and the amino group of urea on the NiFe-LDH surface, while the carbonyl group of urea is preferentially adsorbed on the NiMoP surface. This distribution promotes both OER and UOR processes. Numerous reports suggest that NiFe-LDH-based materials could serve as standalone catalysts for both OER and UOR. However, the problem associated with the NiFe-LDH is poor conductivity. This hinders the superiority of the NiFe-LDH in large-scale applications. To overcome this issue owing to limited charge transport, a promising strategy is to incorporate conductive C materials into the composite. This can enhance the charge transport capabilities of the catalyst, leading to improved overall performance. Moreover, the C support can enhance the catalytic activity by inducing structural changes in the active metal centers through strong interactions. To address this issue, Tavar *et al.* reported an amine-functionalized graphene-rich NiFe-LDH (NiFe-LDH@NH$_2$-G) for the first time as a nanocomposite *via* a one-pot coprecipitation method.[85] NiFe-LDH@NH$_2$-G demands very low overpotentials of 0.41 and 0.32 V *vs.* RHE for the OER and UOR, respectively. Moreover, NiFe-LDH@NH$_2$-G outperforms the activity of bare NiFe-LDH and NiFe-LDH@rGO in both OER and UOR processes. The higher activity after the amination of NiFe-LDH is due to (1) the increase in the carbon/oxygen ratio of the material caused by the removal of oxygen-containing groups and their replacement with amine groups, which facilitates the adsorption of intermediates (OH$^-$ and OOH$^-$) and the electron-accepting nature; (2) the synergistic interaction between Ni and Fe decreases the activation energy and facilitates the charge transport *via* amine-functionalized graphene; (3) the formation of strong Ni^{3+} centers facilitated by the presence of Fe species is the deliberate modification of the electronic structure (Fig. 5e). This structural change leads to the formation of active sites and O$_v$. Hence, the presence of pyridinic-N dopants promotes the adsorption of OER intermediates. Their ability to accept electrons facilitates the formation of OH^{ads} species, leading to improved catalytic performance. However, pristine LDH catalysts

with a loosely hierarchical structure are susceptible to Cl$^-$ adsorption and intercalation between the layers, which can obstruct the active catalytic sites in seawater electrolysis and urea-assisted seawater electrolysis. Based on previous reports, the formation of metal sulfide-LDH heterostructures effectively prevents Cl$^-$-induced corrosion and enhances the OER catalytic activity by providing additional active sites and optimizing the adsorption energy. In view of this report, Boukherroub and his team members developed a heterojunction between the NiFe-LDH and Ni$_3$S$_2$ (NiFe LDH-Ni$_3$S$_2$) as a bifunctional electrocatalyst for seawater splitting, and further used it for the UOR. They adopted a two-step process involving seawater corrosion (presence of Na$^+$ ions) and ion exchange (partial exchange of OH$^-$ groups in the NiFe-LDH with the S^{2-} ion) for the synthesis of NiFe-LDH-Ni$_3$S$_2$ (Fig. 5f). NiFe-LDH-Ni$_3$S$_2$ exhibits 280 mV as overpotential to reach 100 mA cm^{-2} current density in 1 M KOH seawater. Upon further addition of 0.33 M urea to 1 M KOH seawater, the required overpotential decreases to 1.37 V *vs.* RHE to reach the same current density with a difference of 180 mV overpotential compared to KOH without urea (Fig. 5g). The overall urea-assisted seawater splitting requires 1.58 V *vs.* RHE to attain 50 mA cm^{-2} current density for the NiFe-LDH-Ni$_3$S$_2$//NiFe LDH-Ni$_3$S$_2$ system with a long-term stability of 65 h in the same electrolyte, as depicted in Fig. 5h. Hence, the formation of a heterostructure with a sulfide moiety can effectively prevent the Cl$^-$-induced corrosion in seawater electrolysis.[86] In addition to sulfide-based heterostructures, phosphide materials are also promising candidates for coupling with LDHs. Their excellent electrical conductivity, wettability, stability, and applicability across a wide pH range make them an attractive option. The MoP@NiCo-LDH heterostructure, was reported by Zhang *et al.* as a bifunctional electrocatalyst for UOR at the anode and HER at the cathode.[87] The heterostructure was fabricated *via* a three-step hydrothermal process followed by the phosphorization and electrodeposition of NiCo-LDH over the MoP. The LSV polarization in Fig. 5i of urea-water electrolysis (UOR & HER) suggests that the MoP@NiCo-LDH requires a significantly lower voltage (1.405 V) than that of pure water electrolysis (OER and HER) (1.697 V) at a current density of 100 mA cm^{-2}. The two-electrode electrolyzer (MoP@NiCo-LDH/NF-20//MoP@NiCo-LDH/NF-20) operates at a lower cell voltage than that of a Pt/C/NF//IrO$_2$/NF cell. For urea-water electrolysis, the cell voltage is as low as 1.405 V, while for water electrolysis, it is 1.697 V at a current density of 100 mA cm^{-2}. The enhanced performance of the MoP@NiCo-LDH/NF composite is due to its hierarchical structure, which includes a 3D NF framework, MoP, and NiCo-LDH. The hierarchical and 3D structure of the MoP@NiCo-LDH/NF composite facilitates efficient electron transport, thereby improving the electrocatalytic activity for both water and urea electrolysis. In addition to forming p–n or Mott–Schottky heterojunctions, combining LDHs with transition metal halides such as sulfides, selenides, and phosphides offers advantages such as enhanced electrical conductivity, increased active site availability, and inherent electrocatalytic properties. For instance, Hu *et al.* developed a WNiM–WNi LDH (M = Se, S, and p) heterostructured material as a bifunctional electrocatalyst for the OER and UOR.[88] Each of the S-, Se- and P-derived WNi-LDHs exhibits a distinct electrochemical activity towards OER and UOR

processes. For example, the WNiS–WNi LDH requires an overpotential of only 64 mV for the OER, while the WNiP–WNi LDH requires 126 mV for the HER, both at a current density of 10 mA cm^{-2}. Notably, WNiSe–WNi LDH demonstrates exceptional UOR performance, requiring a potential of only 1.25 V to achieve a current density of 10 mA cm^{-2}. The optimized WNiS–WNi LDH anode and WNiP–WNi LDH cathode demonstrate exceptional performance for total water splitting, achieving a current density of 10 mA cm^{-2} at a low cell voltage of 1.45 V in a 1 M KOH solution. Further, WNiS–WNi LDH and WNiP–WNi LDH disclosed a better stability in the OER and HER. However, coming to the UOR, the WNiSe–WNi LDH gets oxidized and forms amorphous oxides/oxyhydroxides over the catalyst surface and poisons the UOR process, which leads to poor stability under the UOR process at high applied potentials. Moreover, the DFT studies demonstrate that the cooperative effect of W and Ni metal ions boosts the charge transfer kinetics and manipulation of electrons within the LDH structure. The robust electronic interaction between the WNi-LDH and P further enhances the redistribution of electrons between W and Ni. This results in enhanced HER catalytic performance. Similarly, the introduction of Se into the WNi-LDH has impact on the adsorption ability of urea intermediates at a higher density and higher Fermi energy levels than those of the WNi-LDH.[88] To address the prior oxidation of selenized Ni-based LDH materials towards the UOR process, Jia and colleagues came up with a material, NiAl-LDH, and selenized it at 450 °C to obtain 4NiAlSe-450.[89] The selenization of NiAl-LDH at 450 °C leads to the formation of mixed-phase NiAl-oxide and NiSe$_2$ as nanoparticles over the layered structure. The *in situ*-grown NiSe$_2$ at 450 °C (4NiAlSe-450) demonstrated superior methanol oxidation reaction (MOR)/UOR electrocatalytic performance, requiring potentials of 1.37 V *vs.* RHE and 1.36 V *vs.* RHE to achieve a current density of 10 mA cm^{-2}, respectively. These values were significantly lower than those of the unmodified NiAl-LDH (1.42 V *vs.* RHE and 1.39 V *vs.* RHE). Further, long-term stability towards the UOR at an applied potential of 1.5 V *vs.* RHE demonstrated stable nature up to 3 h in 1 M KOH + 0.5 M urea. The boosted performance of selenized NiAl-LDH might probably originate from the layered structure, faster electron transfer kinetics due to appropriate selenization and exposure of a large number of active sites as a result of selenization at 450 °C. In conclusion, the fabrication of heterostructures will create a built-in electric field between the two components at the heterointerface owing to discrete energy levels. This built-in electric field enhances the formation of more active sites and effectively regulates the electronic structure of active centers, facilitating electron transfer kinetics during the UOR. Additionally, the selenization of LDH materials enhances and facilitates morphological changes, exposing more active sites for interaction with reagents in the electrolyte. Moreover, selenization significantly improves the electrical conductivity of LDHs, enabling more efficient charge transfer during the UOR process. These combined effects contribute to the enhanced electrocatalytic performance of LDH-based heterostructures for UOR applications. Comparative electrochemical performances of LDH-based electrocatalysts towards urea electrolysis and urea-assisted water splitting are provided in Table 1.

Table 1 Comparison of the electrochemical performances of LDH-based electrocatalysts towards urea electrolysis and water splitting

Sl. no.	Electrocatalyst	UOR				OER				Ref.
		Electrolyte	Cell voltage (V)	Overall water splitting-cell voltage	Current density (mA cm^{-2})	Electrolyte	Cell voltage (V)	Current density (mA cm^{-2})	Overall water splitting- cell voltage	
1	NiFe LDH@Ni(OH)$_2$-z	1 M KOH + 0.5 M urea	1.44	—	100	1 M KOH	1.48	100	—	90
2	Co$_1$Mn$_1$ LDH/NF	1 M KOH + 0.33 M urea	1.38	—	100	1 M KOH	1.48	100	—	91
3	FQD/CoNi-LDH/NF	1 M KOH + 0.5 M urea	1.36	1.45 V@10 mA cm^{-2}	10	1 M KOH	1.598	10	1.59 V@10 mA cm^{-2}	75
5	NiOOH(LDH/α-FeOOH)	1 M KOH + 0.33 M urea	1.37		50	1 M KOH	1.46	50		92
6	MoP@NiCo-LDH/NF-x	1 M KOH + 0.5 M urea	1.392	1.405 V at 100 mA cm^{-2}	100	1 M KOH	1.627	100	1.697 V at 100 mA cm^{-2}	87
7	CoNi-LDH/Fe MOF/NF	1 M KOH + 0.33 M urea	1.37	1.55 V at 100 mA cm^{-2}	100	1 M KOH	1.448	100	1.61 V at 100 mA cm^{-2}	56
8	Hf-NiFe-LDH/NF	1 M KOH + 0.5 M urea	1.37		100	1 M KOH	1.488	100		69
9	NiFeCo LDH/NF	1 M KOH + 0.33 M urea	0.28 *vs.* SCE	1.49 V at 10 mA cm^{-2}	100	1 M KOH	1.44	100	1.57 V at 10 mA cm^{-2}	57
10	NiCoV LDH/NF	1 M KOH + 0.33 M urea	1.33	1.45 V at 10 mA cm^{-2}	10	1 M KOH	1.60	10	1.66 V at 10 mA cm^{-2}	58
11	NiCo$_2$S$_4$@NiMn LDH	1 M KOH + 0.33 M urea	1.37		100	1 M KOH		100		54
12	Zr–NiFe LDH@NiFe$_2$O$_4$/NF	1 M KOH + 0.33 M urea	~1.41		50	1 M KOH		50		93
13	ZnCoFeS-LDH	1 M KOH + 0.33 M urea	1.398		100	1 M KOH	1.491	100		94
14	NiFe-LDH/MWCNTs/NF	1 M KOH + 0.5 M urea	1.4	1.507 V at 10 mA cm^{-2}	100	1 M KOH	1.662	100	1.663 V at 10 mA cm^{-2}	95
15	NiFe LDH/MoS$_2$/Ni$_3$S$_2$/NF	1 M KOH + 0.5 M urea	1.410		50	1 M KOH	1.51	50		78
16	CuCo$_2$O$_4$@ACoNi-LDH	1 M KOH + 0.5 M urea	1.292		10	1 M KOH	1.429	10		96
17	Sn-NiFe LDH/NF	1.5 M KOH + 0.5 M urea	1.35		10	1 M KOH	1.49	10		72

In this context, it is worth mentioning that LDH materials are well known for the OER process. Various structural and electronic modifications were also reported to enhance the OER performance.[22] The main purpose of these structural and electronic tunings of the LDH material for the OER is to optimize the adsorption/desorption phenomena of the reaction intermediates ((*OH/*O/*OOH), for better catalytic performance. On the contrary, the main purpose of tuning the LDH material for the UOR is to increase the selectivity of the catalyst towards urea adsorption and promote the formation of intermediates such as *CO and *NCO, apart from optimizing their parameters such as active surface area and electronic conductivity. Hence, more focus and strategic designs are required to do the structural and electronic modification of LDHs for urea oxidation reactions, which is our topic of interest. Moreover, the gap between the theoretical potential for the UOR and OER is 0.86 V. Hence, at a low anodic potential, the UOR is not a competitor for the OER, but rather a sacrificial agent which requires less energy input. Hence, a highly selective and optimized LDH structure could deliver the desired high current density at low anodic potentials without going to the potential range of OERs to avoid competition. The comparison of LDH materials for UORs and OERs at different operating voltages is presented in Table 1 for better understanding.

6.5. *In situ* understanding of the structural features of LDHs during UORs

Despite the thermodynamic and kinetic aspects associated with water oxidation, a significant progress has been achieved in recent years with the development of both molecular catalysts and oxide-based materials. While molecular redox catalysts offer potential advantages, their catalytic cycles often involve multiple oxidation states, which, coupled with the harsh reaction conditions, can lead to catalyst degradation. However, this dynamic environment can also facilitate the *in situ* formation of new and sometimes superior catalytic species. Recently, numerous reports have showcased *in situ*-generated molecular complexes and metal-oxide catalysts exhibiting high activity for water oxidation reactions. Consequently, a precise understanding of the structural and electronic changes of catalysts during oxidative activation is crucial. This knowledge is essential for identifying the nature (single-site or multi-site) and structure of the true active species, elucidating its reaction mechanism, and ultimately enabling the rational design and improvement of more efficient catalysts.[97] Recently, Tang *et al.* have synthesized an ultrathin nanoflower-like S-NiFeLDH/MXene over the NF, where they employed *in situ* Raman analysis to elucidate the structural transformation for the higher OER and UOR performance.[79] S-NiFe LDH/MXene@NF demonstrated electrocatalytic activities for OER and UOR with potentials of 1.578 V and 1.437 V *vs.* RHE, respectively at a current density of 500 mA cm^{-2}. The *in situ* Raman analysis at lower potentials (1.25–1.30 V *vs.* RHE) revealed the appearance of peaks at 460 and 1003 cm^{-1}, corresponding to Ni^{2+}–OH vibrations and the N–C–N bond of urea, respectively. Upon increasing the potential to 1.325 V *vs.* RHE, a new peak emerged

at 528 cm^{-1}, attributed to Ni^{2+}–O vibrations, suggesting the onset of surface oxidation. Further increasing the potential beyond 1.35 V *vs.* RHE resulted in the appearance of new signals at 475 and 555 cm^{-1}, attributed to the Ni^{3+}–O bending and stretching vibrations in NiOOH. The evolution of these Raman peaks provides direct evidence for the *in situ* oxidation of Ni(OH)$_2$ to NiOOH on the catalyst surface. This *in situ* oxidation of Ni(OH)$_2$ to NiOOH coincides with the onset of urea oxidation (1.35 V *vs.* RHE) during the positive sweep contributing to the enhanced UOR activity. Similarly, Wu *et al.* demonstrate that doping of Mn in Ni(OH)$_2$ lowers the onset potential for Ni(OH)$_2$ oxidation.[70] This facilitates the formation of electrochemically active Ni^{3+} OOH and enhances the electrochemical reversibility of the Ni redox couple within the NiMn-LDH. *In situ* Raman spectroscopy revealed the surface transformations of the catalyst during the UOR. In 1 M KOH, the initial Raman spectra exhibited peaks at 455 and 500 cm^{-1}, corresponding to Ni^{2+}–OH vibrations in Ni(OH)$_2$. Upon increasing the potential to 0.38 V, a new peak emerged at 556 cm^{-1}, suggesting the formation of NiOOH. At higher potentials (> 0.40 V), the spectra exhibited a doublet at 479 and 561 cm^{-1}, confirming the formation of NiOOH. The presence of a broad feature in the 900–1150 cm^{-1} region at higher potentials suggested the formation of superoxide species within the NiOOH structure. In the case of 0.33 M urea, they observed a similar spectral property. However, the onset of NiOOH formation occurred at a slightly lower potential (0.38 V). A new peak around 1004 cm^{-1}, attributed to the symmetric C–N stretching of urea, gets degraded at higher potentials, probably due to the disruption of bubble formation at higher potential. These *in situ* Raman spectroscopic studies provide direct evidence for the *in situ* formation of NiOOH as the active phase for urea oxidation, which is correlated with the observed electrochemical behavior. In summary, *in situ* Raman analysis offers valuable insights and a clear mechanistic explanation for the critical roles of electrocatalysts in enhancing the performance of oxidation reactions.

7. Current challenges and future perspectives in UORs

Electrochemical UOR is a crucial, energy-efficient half-reaction for urea-assisted H$_2$ production, offering a sustainable alternative. However, its slower kinetics presents a great challenge that needs to be addressed:

(1) First, the development of more efficient and durable catalysts is the most vital area for future research in UOR-assisted H$_2$ generation. The focus here would be on catalysts with improved surface properties, enhanced active-site exposure, and better electronic conductivity. Modifications such as doping, and creating defect-rich surfaces or heterostructures, including unexplored materials over the LDH would inherently boost the kinetically sluggish process. The activity and stability of multicomponent transition metal LDHs also show synergistic effects resulting from the combination of metal centers.

(2) Second, selectivity and by-product formation-complex reaction pathways in the UOR can result in undesired

by-products, which include ammonia and nitrate. These by-products complicate the reaction and lower the purity of the H_2 produced. Selectivity control of unwanted products such as ammonia or nitrates is a serious challenge that requires further interest. Further, the qualitative and quantitative understanding of UOR by products will provide a path to study the reaction mechanism. Hence, tailoring catalysts to favor the desired reaction pathways and optimize the production of high-purity H_2 will be key to making UOR more viable for industrial applications.

(3) Third, mechanistic insights and theoretical modeling of the intermediates and rate-limiting steps in the detailed reaction mechanisms of UOR are still unidentified. This lack of insight limits the rational design of more effective catalysts. Improvements in catalyst design require a deeper understanding of the UOR reaction pathway. Exploring the mechanisms and identifying the active intermediates and the rate-limiting steps by using *in situ/operando* spectroscopic techniques and advanced computational modeling will lead to more targeted material design.

(4) Finally, device integration and scaling up laboratory-based UOR technologies to industrial applications are quite challenging. The future direction has to be the integration of UOR catalysts in practical devices such as urea-based fuel cells, urea electrolysis systems, or in wastewater treatment plants. Efforts could be made to optimize the electrode designs, improve the mass transport, and formulate scalable, cost-effective manufacturing process for the development of highly efficient and durable electrode materials capable of being integrated into realistic hydrogen production. Overcoming these challenges would make UOR significant players in achieving cleaner production of energy and environmental sustainability.

8. Summary

This review comprehensively examined LDHs as urea oxidation electrocatalysts, moving beyond mere systematics summarized by investigating into the intricate relationship between their composition, structure, and catalytic activity. Further, it highlighted significant advancements in the design and synthesis of UOR catalysts achieved through recent progress with LDHs, showcasing a critical analysis of strategies employed in catalyst design. These strategies include introducing surface defects, intercalating anions and cations, forming hybrids or heterostructures with other materials, doping with noble or non-noble metals or nanoparticles, tuning the morphology of LDH, increasing the surface area, introducing new active sites, each of which significantly improves the structural and electronic properties of LDH-based materials. Moreover, this review focused on structure-effect relationships, product selectivity, UOR-OER competition, and reaction pathways. Building upon the advancements in various UOR electrocatalysts, it further outlines the future design strategies and emphasizes the key challenges that still persist. We believe this article provides innovative insights into the different mechanisms of UORs, thereby inspiring the development of innovative materials to have significant impacts the future energy landscape.

References

1 Y. Li, X. Wei, L. Chen and J. Shi, *Angew. Chem., Int. Ed.*, 2021, **60**, 19550–19571.
2 M. S. Dresselhaus and I. L. Thomas, *Nature*, 2001, **414**, 332–337.
3 B. Zhu, Z. Liang and R. Zou, *Small*, 2020, **16**, 1–19.
4 X. Gao, S. Zhang, P. Wang, M. Jaroniec, Y. Zheng and S. Z. Qiao, *Chem. Soc. Rev.*, 2024, **53**, 1552–1591.
5 R. K. Singh, K. Rajavelu, M. Montag and A. Schechter, *Energy Technol.*, 2021, **9**, 1–28.
6 J. Li, S. Wang, J. Chang and L. Feng, *Adv. Powder Mater.*, 2022, **1**, 100030.
7 Y. Isaka, S. Kato, D. Hong, T. Suenobu, Y. Yamada and S. Fukuzumi, *J. Mater. Chem. A*, 2015, **3**, 12404–12412.
8 K. Ye, G. Wang, D. Cao and G. Wang, *Top. Curr. Chem.*, 2018, **376**, 42.
9 G. Gnana Kumar, A. Farithkhan and A. Manthiram, *Adv. Energy Sustainability Res.*, 2020, **1**, 1–17.
10 L. M. Le Leuch and T. J. Bandosz, *Carbon*, 2007, **45**, 568–578.
11 S. D. Yim, S. J. Kim, J. H. Baik, I. S. Nam, Y. S. Mok, J. H. Lee, B. K. Cho and S. H. Oh, *Ind. Eng. Chem. Res.*, 2004, **43**, 4856–4863.
12 Y. Li, H. Wang, R. Wang, B. He and Y. Gong, *Mater. Res. Bull.*, 2018, **100**, 72–75.
13 C. Zequine, F. Wang, X. Li, D. Guragain, S. R. Mishra, K. Siam, P. K. Kahol and R. K. Gupta, *Appl. Sci.*, 2019, **4**, 9.
14 S. Anantharaj, S. R. Ede, K. Sakthikumar, K. Karthick, S. Mishra and S. Kundu, *ACS Catal.*, 2016, **6**, 8069–8097.
15 R. Madhu, A. Karmakar, K. Bera, S. Nagappan, H. N. Dhandapani, A. De, S. S. Roy and S. Kundu, *Mater. Chem. Front.*, 2023, **7**, 2120–2152.
16 J. Li, C. Yin, S. Wang, B. Zhang and L. Feng, *Chem. Sci.*, 2024, **15**, 13659–13667.
17 C. Yin, F. Yang, S. Wang and L. Feng, *Chin. J. Catal.*, 2023, **51**, 225–236.
18 J. Li, S. Sun, Y. Yang, Y. Dai, B. Zhang and L. Feng, *Chem. Commun.*, 2022, **58**, 9552–9555.
19 S. Song, X. Huang, Y. Yang and L. Feng, *Chem. Commun.*, 2024, **2**, 10906–10909.

20 S. Jiang, M. Zhang, C. Xu, G. Liu, K. Zhang, Z. Zhang, H. Q. Peng, B. Liu and W. Zhang, *ACS Nano*, 2024, **18**, 16413–16449.

21 T. A. Saleh, *Nano-Struct. Nano-Objects*, 2024, **37**, 101109.

22 A. Karmakar, K. Karthick, S. S. Sankar, S. Kumaravel, R. Madhu and S. Kundu, *J. Mater. Chem. A*, 2021, **9**, 1314–1352.

23 Y. Wang, D. Yan, S. El Hankari, Y. Zou and S. Wang, *Adv. Sci.*, 2018, **5**, 1800064.

24 S. Lu, X. Zheng, L. Fang, F. Yin and H. Liu, *Electrochem. Commun.*, 2023, **157**, 107599.

25 J. Tang, Z. Li, H. Jang, X. Gu, C. Sun, M. G. Kim, L. Hou and X. Liu, *Adv. Energy Mater.*, 2024, **2403004**, 1–8.

26 J. M. Huo, Y. Wang, J. N. Xue, W. Y. Yuan, Q. G. Zhai, M. C. Hu, S. N. Li and Y. Chen, *Small*, 2024, **20**, 1–9.

27 M. Zeng, J. Wu, Z. Li, H. Wu, J. Wang, H. Wang, L. He and X. Yang, *ACS Sustainable Chem. Eng.*, 2019, **7**, 4777–4783.

28 P. Li, W. Li, Y. Huang, Q. Huang, J. Li, S. Zhao and S. Tian, *ChemSusChem*, 2023, **16**, e202201921.

29 J. Zhang, X. Song, L. Kang, J. Zhu, L. Liu, Q. Zhang, D. J. L. Brett, P. R. Shearing, L. Mai, I. P. Parkin and G. He, *Chem. Catal.*, 2022, **2**, 3254–3270.

30 T. Zhou, S. N. Jagadeesan, L. Zhang, N. A. Deskins and X. Teng, *J. Phys. Chem. Lett.*, 2024, **15**, 81–89.

31 M. A. Hefnawy, S. A. Fadlallah, R. M. El-Sherif and S. S. Medany, *J. Alloys Compd.*, 2022, **896**, 162857.

32 R. P. Forslund, C. T. Alexander, A. M. Abakumov, K. P. Johnston and K. J. Stevenson, *ACS Catal.*, 2019, **9**, 2664–2673.

33 X. Sun and R. Ding, *Catal. Sci. Technol.*, 2020, **10**, 1567–1581.

34 C. Lamy and P. Millet, *J. Power Sources*, 2020, **447**, 227350.

35 C. Zhen, W. Wei, H. K. Shon and B. J. Ni, *Green Chem.*, 2023, **26**, 631–654.

36 C. J. Huang, H. M. Xu, T. Y. Shuai, Q. N. Zhan, Z. J. Zhang and G. R. Li, *Small*, 2023, **19**, 2301130.

37 W. Ge, L. Lin, S. Q. Wang, Y. Wang, X. Ma, Q. An and L. Zhao, *J. Mater. Chem. A*, 2023, **11**, 15100–15121.

38 D. Zhu, H. Zhang, J. Miao, F. Hu, L. Wang, Y. Tang, M. Qiao and C. Guo, *J. Mater. Chem. A*, 2022, **10**, 3296–3313.

39 S. Xu, X. Ruan, M. Ganesan, J. Wu, S. K. Ravi and X. Cui, *Adv. Funct. Mater.*, 2024, **34**, 1–35.

40 E. Urbańczyk, M. Sowa and W. Simka, *J. Appl. Electrochem.*, 2016, **46**, 1011–1029.

41 A. Zaher and N. Shehata, *IOP Conf. Ser.: Mater. Sci. Eng.*, 2021, **1046**, 012021.

42 H. Zöllig, A. Remmele, C. Fritzsche, E. Morgenroth and K. M. Udert, *Environ. Sci. Technol.*, 2015, **49**, 11062–11069.

43 K. Cho, D. Kwon and M. R. Hoffmann, *RSC Adv.*, 2014, **4**, 4596–4608.

44 D. A. Daramola, D. Singh and G. G. Botte, *J. Phys. Chem. A*, 2010, **114**, 11513–11521.

45 M. Siyata, *Clays Clay Miner.*, 1975, **23**, 369–375.

46 M. R. Berber, I. H. Hafez, K. Minagawa, M. Katoh, T. Mori and M. Tanaka, *J. Mol. Struct.*, 2013, **1033**, 104–112.

47 H. N. Dhandapani, D. Mahendiran, A. Karmakar, P. Devi, S. Nagappan, R. Madhu, K. Bera, P. Murugan, B. R. Babu and S. Kundu, *J. Mater. Chem. A*, 2022, **10**, 17488–17500.

48 J. Prince, A. Montoya, G. Ferrat and J. S. Valente, *Chem. Mater.*, 2009, **21**, 5826–5835.

49 O. Bergadà, I. Vicente, P. Salagre, Y. Cesteros, F. Medina and J. E. Sueiras, *Microporous Mesoporous Mater.*, 2007, **101**, 363–373.

50 B. Sang, Y. Liu, X. Wan, S. Xie, G. Zhang, M. Ge, J. Dai, W. Zhang and R. Q. Li, *Chem. Commun.*, 2023, **59**, 8743–8746.

51 J. Li, J. Zhang and J. H. Yang, *Int. J. Hydrogen Energy*, 2022, **47**, 7693–7712.

52 Z. Wang, W. Liu, Y. Hu, M. Guan, L. Xu, H. Li, J. Bao and H. Li, *Appl. Catal., B*, 2020, **272**, 118959.

53 Y. Ding, X. Du and X. Zhang, *Appl. Surf. Sci.*, 2022, **584**, 152622.

54 K. Peng, N. Bhuvanendran, F. Qiao, G. Lei, S. Y. Lee and H. Su, *ACS Appl. Nano Mater.*, 2023, **6**, 18318–18327.

55 T. X. Nguyen, Z. Y. Wei, T. M. Zheng, Y. H. Su, K. S. Chuang and J. M. Ting, *Chem. Eng. J.*, 2024, **496**, 153841.

56 Q. N. Bian, B. S. Guo, D. X. Tan, D. Zhang, W. Q. Kong, C. Bin Wang and Y. Y. Feng, *ACS Appl. Mater. Interfaces*, 2024, **16**, 14742–14749.

57 P. Babar, A. Lokhande, V. Karade, B. Pawar, M. G. Gang, S. Pawar and J. H. Kim, *ACS Sustainable Chem. Eng.*, 2019, **7**, 10035–10043.

58 J. Guo, H. Zhang, Y. Yang, M. Wei and H. Zhang, *J. Mater. Chem. A*, 2024, **12**, 16780–16792.

59 L. Wang, Y. Zhu, Y. Wen, S. Li, C. Cui, F. Ni, Y. Liu, H. Lin, Y. Li, H. Peng and B. Zhang, *Angew. Chem.*, 2021, **133**, 10671–10676.

60 R. P. Forslund, J. T. Mefford, W. G. Hardin, C. T. Alexander, K. P. Johnston and K. J. Stevenson, *ACS Catal.*, 2016, **6**, 5044–5051.

61 G. Liu, C. Huang, Z. Yang, J. Su and W. Zhang, *Appl. Catal., A*, 2021, **614**, 118049.

62 D. Li, X. Zhou, L. Liu, Q. Ruan, X. Zhang, B. Wang, F. Xiong, C. Huang and P. K. Chu, *Appl. Catal., B*, 2023, **324**, 122240.

63 P. F. Liu, S. Yang, B. Zhang and H. G. Yang, *ACS Appl. Mater. Interfaces*, 2016, **8**, 34474–34481.

64 H. Li, Q. Yu, X. Zhu, H. Wu, Z. Dai, L. Li, W. Zhu, S. Li and Z. Chen, *Chem. Eng. J.*, 2024, **493**, 152860.

65 L. Chen, H. Wang, L. Tan, D. Qiao, X. Liu, Y. Wen, W. Hou and T. Zhan, *J. Colloid Interface Sci.*, 2022, **618**, 141–148.

66 S. Xu, D. Jiao, X. Ruan, Z. Jin, Y. Qiu, Z. Feng, L. Zheng, J. Fan, W. Zheng and X. Cui, *Adv. Funct. Mater.*, 2024, **2401265**, 1–11.

67 G. Liu, C. Xie, Y. Zhang, Y. Du, J. Wang, J. Lin, J. Bai, J. Li, C. Zhou, T. Zhou and B. Zhou, *J. Colloid Interface Sci.*, 2024, **668**, 375–384.

68 D. Khalafallah, L. Xiaoyu, M. Zhi and Z. Hong, *ChemElectroChem*, 2020, **7**, 163–174.

69 J. Wang, M. Wang, Z. Lu, J. Xie, J. Huang, J. Hu and Y. Cao, *Int. J. Hydrogen Energy*, 2024, **82**, 724–732.

70 X. Yang, H. Zhang, W. Xu, B. Yu, Y. Liu and Z. Wu, *Catal. Sci. Technol.*, 2022, **12**, 4471–4485.

71 Z. Wang, W. Liu, J. Bao, Y. Song, X. She, Y. Hua, G. Lv, J. Yuan, H. Li and H. Xu, *Chem. Eng. J.*, 2022, **430**, 133100.

72 X. Zhang, X. Wu and X. Du, *New J. Chem.*, 2024, **48**, 7856–7862.

73 H. Sun, W. Zhang, J. G. Li, Z. Li, X. Ao, K. H. Xue, K. K. Ostrikov, J. Tang and C. Wang, *Appl. Catal., B*, 2021, **284**, 119740.

74 K. Wang, M. Hou, W. Huang, Q. Cao, Y. Zhao, X. Sun, R. Ding, W. Lin, E. Liu and P. Gao, *J. Colloid Interface Sci.*, 2022, **615**, 309–317.

75 Y. Feng, X. Wang, J. Huang, P. Dong, J. Ji, J. Li, L. Cao, L. Feng, P. Jin and C. Wang, *Chem. Eng. J.*, 2020, **390**, 124525.

76 J. Guan, X. Li, Y. Zhu, Y. Dai, R. Zhang, B. Guo and M. Zhang, *New J. Chem.*, 2023, **47**, 16964–16971.

77 X. Yan, Q. T. Hu, G. Wang, W. Da Zhang, J. Liu, T. Li and Z. G. Gu, *Int. J. Hydrogen Energy*, 2020, **45**, 19206–19213.

78 C. Li, T. Yang, J. Fan, E. Liu, B. Zhao and T. Sun, *J. Alloys Compd.*, 2024, **970**, 172710.

79 Y. Liu, X. Hong, X. Liu, W. Chen and J. Tang, *ACS Sustainable Chem. Eng.*, 2024, **12**, 11520–11530.

80 M. H. Sepahdar, S. M. Masoudpanah, M. S. Bafghi, M. Mehri and B. Aslibeiki, *Int. J. Hydrogen Energy*, 2024, **85**, 733–743.

81 T. Song, H. Xue, J. Sun, N. Guo, J. Sun, Y. R. Hao and Q. Wang, *Chem. Commun.*, 2023, **60**, 972–975.

82 S. Qiao, C. Rao, H. Chen, M. Xiong, Q. Xu and S. Ci, *J. Alloys Compd.*, 2024, **1004**, 175823.

83 X. Zhang, J. Zhang, Z. Ma, L. Wang, K. Yu, Z. Wang, J. Wang and B. Zhao, *J. Colloid Interface Sci.*, 2024, **665**, 313–322.

84 L. Wei, L. Zhang, L. Li and J. Su, *Int. J. Hydrogen Energy*, 2024, **82**, 64–72.

85 D. Tavar, S. K. Ojha, Z. Zaidi, H. Prasad, R. K. Sharma, M. Ashiq, M. Mudgal and A. Singh, *ACS Appl. Nano Mater.*, 2023, **6**, 22517–22531.

86 Z. H. Zhang, Z. R. Yu, Y. Zhang, A. Barras, A. Addad, P. Roussel, L. C. Tang, M. Naushad, S. Szunerits and R. Boukherroub, *J. Mater. Chem. A*, 2023, **11**, 19578–19590.

87 T. Wang, H. Wu, C. Feng, L. Zhang and J. Zhang, *J. Mater. Chem. A*, 2020, **8**, 18106–18116.

88 C. Zhang, X. Du, X. Zhang, Y. Wang and T. Hu, *Dalton Trans.*, 2023, **52**, 6052–6060.

89 X. Wang, J. Wang, A. Xu, Y. Chang, J. Jia and M. Jia, *Int. J. Hydrogen Energy*, 2023, **48**, 22060–22068.

90 Y. Ye, Y. Gan, R. Cai, X. Dai, X. Yin, F. Nie, Z. Ren, B. Wu, Y. Cao and X. Zhang, *J. Alloys Compd.*, 2022, **921**, 166145.

91 F. Miao, P. Cui, T. Gu, S. Yu, Z. Yan and G. Hai, *Dalton Trans.*, 2023, **53**, 1599–1606.

92 M. Cai, Q. Zhu, X. Wang, Z. Shao, L. Yao, H. Zeng, X. Wu, J. Chen, K. Huang and S. Feng, *Adv. Mater.*, 2023, **35**, 1–10.

93 W. Wen, X. Du and X. Zhang, *Int. J. Hydrogen Energy*, 2024, **81**, 615–623.

94 R. Li, D. Zhang, H. Chen, S. Wang, Y. Ling and C. Fang, *ACS Sustain. Chem. Eng.*, 2023, **11**, 16098–16107.

95 X. Wen, *Int. J. Hydrogen Energy*, 2020, **45**, 14660–14668.

96 Y. Wang, P. Li, X. Du and X. Zhang, *Int. J. Hydrogen Energy*, 2024, **54**, 937–946.

97 K. S. Joya and X. Sala, *Phys. Chem. Chem. Phys.*, 2015, **17**, 21094–21103.